

VYSOKÁ ŠKOLA BÁŇSKÁ - TECHNICKÁ UNIVERZITA OSTRAVA
UNIVERZITNÍ STUDIJNÍ PROGRAMY
NANOTECHNOLOGIE

Modeling of plasmonic nanostructures in COMSOL

Modelování plasmonických nanostruktur
v prostředí COMSOL

student: Bc. Barbora Kacerovská

supervisor: Ing. Jan Chochol



Diploma Thesis

2017

Diploma Thesis Assignment

Student: **Bc. Barbora Kacerovská**

Study Programme: N3942 Nanotechnology

Study Branch: 3942T001 Nanotechnology

Title: **Modeling of plasmonic nanostructures in COMSOL**
Modelování plazmonických nanostruktur v prostředí COMSOL

The thesis language: English

Description:

Finite element method (FEM) is used to solve the behavior of electromagnetic (EM) waves in various structures. COMSOL is widely used commercial software solving range of problems by application of FEM.

Guiding electromagnetic waves on the boundary between metal and dielectric is called the surface plasmon polariton (SPP). The light is concentrated into smaller area than the diffraction limit and this effect is extremely sensitive to changes in materials. The use of SPP lies mainly in sensor technology. Another possible use is in integrated optics for construction of smaller and faster photonic chips where light is guided by surface plasmon waveguides (i.e. metal-insulator-metal architecture).

Main targets of the master thesis are summarized in the following points:

- physical description of the surface plasmon polaritons
- description of finite element method and the use of boundary conditions
- verification of calculation on known 2D structures
- modeling of advanced plasmonic nanostructures.

References:

Yeh, P. Optics of anisotropic layered media: A new 4×4 matrix algebra. *Surface Science* 41–53 (1980). doi:10.1016/0039-6028(80)90293-9.

Raether, H. *Surface Plasmons on Smooth and Rough Surfaces and on Gratings*. 111, (Springer Berlin Heidelberg, 1988).

COMSOL Multiphysics User's guide [online].

JIN, Jian-Ming. *The finite element method in electromagnetics*. New York: Wiley, c1993. ISBN 0-471-58627-7.

Berini, P. Long-range surface plasmon polaritons. *Advances in Optics and Photonics* 1, 484 (2009).


Extent and terms of a thesis are specified in directions for its elaboration that are opened to the public on the web sites of the faculty.

Supervisor: **Ing. Jan Chochol**


Consultant: doc. Dr. Mgr. Kamil Postava

Date of issue: 20.10.2016

Date of submission: 15.05.2017



prof. Ing. Jaromír Pištora, CSc.
Head of Department



prof. Ing. Petr Noskievič, CSc.
Vice-rector for Study Affairs



Prohlášení

- Byla jsem seznámena s tím, že na moji diplomovou práci se plně vztahuje zákon č.121/2000 Sb. - autorský zákon, zejména § 35 - využití díla v rámci občanských a náboženských obřadů, v rámci školních představení a využití díla školního a § 60 – školní dílo.
- Beru na vědomí, že Vysoká škola báňská - Technická univerzita Ostrava (dále jen VŠB-TUO) má právo nevýdělečně, ke své vnitřní potřebě, diplomovou práci užít (§ 35 odst. 3).
- Souhlasím s tím, že jeden výtisk diplomové práce bude uložen v Ústřední knihovně VŠB-TUO k prezenčnímu nahlédnutí a jeden výtisk bude uložen u vedoucího diplomové práce. Souhlasím s tím, že údaje o diplomové práci, obsažené v Záznamu o závěrečné práci, umístěném v příloze mé diplomové práce, budou zveřejněny v informačním systému VŠB-TUO.
- Bylo sjednáno, že s VŠB-TUO, v případě zájmu z její strany, uzavřu licenční smlouvu s oprávněním užití díla v rozsahu § 12 odst. 4 autorského zákona.
- Bylo sjednáno, že užít své dílo – diplomovou práci, nebo poskytnout k licenci k jejímu využití mohu jen se souhlasem VŠB-TUO, která je oprávněna v takovém případě ode mě požadovat přiměřený příspěvek na úhradu nákladů, které byly VŠB-TUO na vytvoření díla vynaloženy (až do jejich skutečné výše).
- Místopřísežně prohlašuji, že celou diplomovou práci včetně příloh jsem vypracovala samostatně a uvedla jsem všechny použité podklady a literaturu.

Declaration

I declare I elaborated this thesis by myself. All literary sources and publications I have used had been cited.

Ostrava, May 15, 2017

Abstrakt

Pro řešení a popis chování elektromagnetických vln v různých strukturách je často používaná metoda konečných prvků (MKP). Software COMSOL Multiphysics řeší pomocí MKP široké spektrum fyzikálních úloh. Vedená elektromagnetická vlna na rozhraní mezi kovem a dielektrikem se nazývá povrchový plasmon polariton. Světlo je koncentrováno do oblasti, která je menší než difrakční limit, a jeho chování je silně závislé na změnách v materiálu. Povrchové plasmony jsou nejvíce využívány v oblasti senzorů, popřípadě v integrované optice pro konstrukci malých a rychlých fotonických čipů, kde je světlo vedeno pomocí plasmonických vlnodů (např. architektura kov - izolátor - kov).

Tato diplomová práce by měla čtenáři poskytnout základní informace o plasmonice a především o možnostech modelování 2D plasmonických nanostruktur pomocí softwaru COMSOL Multiphysics. Práce obsahuje několik příkladů, na kterých jsou ukázány základní postupy při modelování. Jako pokročilé struktury jsme zvolili struktury využívající magnetooptické jevy.

Klíčová slova: povrchový plasmon polariton, COMSOL Multiphysics, RF module, plasmonický vlnod, elektromagnetismus

Abstract

Finite element method (FEM) is used to solve the behavior problem of electromagnetic (EM) waves in various structures. COMSOL is widely used commercial software solving range of problems by application of FEM. Guided electromagnetic waves on the boundary between metal and dielectric is called the surface plasmon polariton (SPP). The light is concentrated into smaller area than the diffraction limit and this effect is extremely sensitive to changes in materials. The use of SPP lies mainly in sensor technology. Another possible use is in integrated optics for construction of smaller and faster photonic chips where light is guided by surface plasmon waveguides (e.g. metal-insulator-metal architecture).

This diploma thesis should provide the reader with the fundamentals of the plasmonics and especially the possibilities of modeling 2D nanostructures in COMSOL Multiphysics software. The thesis contains several model examples on which the modeling process is shown. As advanced nanostructures we choose the nanostructures that use magneto-optics effects.

Keywords: surface plasmon polariton, COMSOL Multiphysics, RF module, plasmonic waveguide, electromagnetism

Acknowledgements

Writing the diploma thesis has had a big impact on me. It has been a long period of intense learning and I would like to express my gratitude to the people that have helped me and encouraged me.

First and foremost, I would like to thank my thesis supervisor Ing. Jan Chochol who has supported me throughout the writing with his patience and knowledge. He consistently allowed this thesis to be my own work but steered me in the right direction whenever I needed it. The thesis would not have been accomplished without his guidance. One simply could not wish for a better supervisor.

I also thank my consultant doc. Dr. Mgr. Kamil Postava who has introduced me to the optics and helped me to find the theme of my diploma thesis and RNDr. Dalibor Ciprian PhD. for consultation and good tips for modeling in COMSOL Multiphysics.

In my daily work I have been blessed with my friendly fellow students. Tomáš Kohut, who helped me get on the road to MATLAB and L^AT_EX , Zuzana Grosmanová, who provided me with an experienced ear for my doubts about writing the thesis, and Lukáš Sojka, who has the best sense of humor and can lighten every possible situation.

My best friend Jiří Pavlásek always found a time for me and pushed me and encouraged me when it was necessary. I hope he will read this thesis to find out that the plasmon is not a small mystical creature called "Plašmoň" and that I really do physics.

I am deeply thankful to my parents for unremittingly supporting me throughout the whole study. Without them this thesis would not have been possible.

Finally, there is my partner Michal. I am so thankful that I have him, especially in the final months of my study which were the hardest.

Thank you very much, everyone!

Contents

1	Introduction	1
1.1	Organization of the thesis	6
2	Electromagnetics Background	7
2.1	Maxwell's equations	7
2.2	Reflection of a plane wave and polarization modes	9
	Thin-film interference	12
2.3	Fundamentals of surface plasmons	13
2.4	Material properties	16
	Lorentz oscillator	16
	Drude model for free electrons	18
	Drude-Lorentz model	20
	Permittivity	20
3	Finite Element Method in COMSOL Multiphysics	23
3.1	Basic principles of FEM	23
3.2	Weak formulation of a waveguide	25
3.3	Modeling in COMSOL Multiphysics	26
4	Surface Plasmon Resonance	29
4.1	Kretschmann-Raether configuration	29
4.2	Otto configuration	36
	Otto configuration with external magnetic field	38
5	Plasmonic Waveguides	40
5.1	Planar waveguides	40
5.2	Metal cylinder waveguides	44
	Metal cylinder waveguide with external magnetic field	49
6	Conclusion	52

1 Introduction

Classical optics stretches into prehistory and is one of the oldest fields of human inquiry. Its subdisciplines micro and nanooptics are at best century old and most of these fields developed significantly at the beginning of the 21st century. Present-day applications range from medicine to entertainment and are widely used in a day-life. Optical devices are known from the dawn history: the Babylonians used lenses made from quartz, Egyptian had mirrors (1200 BCE) and similar technologies were found by archaeologists all over the world. The Lycurgus cup from Byzantine empire dating back to the 4th century A.D. shown in Figure 1.1 appears green under normal lighting, however, when illuminated from within it becomes vibrant red in colour. The effect is the consequence of a presence of tiny proportions of gold and silver nanoparticles dispersed in colloidal form throughout the glass material. This phenomenon was not described properly until the 20th century and today we called this effect plasmonic excitations and it is part of nanooptics [1].



Figure 1.1: The Lycurgus cup illuminated under normal external lighting (left) and from within (right) [1].

As scientific and engineering developments have made the micro and nano worlds more accessible, new aspects of optics have come to light and nanooptics has considerable promise for novel and still unknown science and engineering. Field that represents the convergence of microoptics, photonics, nanooptics and nanotechnology is called nanophotonics and is expected to yield significant technical and scientific impact. One of the developments of the late 20th century of the nanophotonics is the photonic crystal, which is a spatially repeating structure with periods in the sub-wavelength regime, so, as a result, the photonics crystal can exhibit a photonic band gap, and the transmission of photons in certain energy ranges is inhibited in it. These crystals are employed for enhancing the emission of microoptical light emitters, waveguides with interesting dispersive properties, excellent mirrors for wide

range of wavelengths or photonic crystal fibers. Moreover, new nanophotonics studies are also focusing on the development of metamaterials - structured media not found in nature, often with customizable propagation characteristics. A very attractive property that can be realized is the negative index of refraction. Lenses based on this property can also focus the evanescent field and may result in a perfect focus, beyond the diffraction limit; in the future we can invent invisibility cloak, which bends light around an object such that it is not visible to an observer [2].

Another great field of nanophotonics is plasmonics. It represents one of the most active research areas at the interface of nanophysics and optics. Plasmon is quasiparticle which is characterized as the quantized collective excitation of electrons and is typically found at the surface of metals. It consists of charges that interact with an electromagnetic field and may be highly localized and propagate along the surface. The electromagnetic field is tightly concentrated at the surface and decay exponentially in the surface-normal direction. Essential for the generation of surface plasmons (SPs) is the presence of free electrons at the interface of two materials which in practice means that one of these materials is conductive. That implies that surface plasmons can be considered as propagating electron density waves occurring at the interface between metal and dielectric or SPs can be viewed as electromagnetic waves strongly bound to this interface [3].

The use of plasmons in optics is not new. The first studies in which surface plasmons were observed date back to the beginning of the 20th century. In 1902 prof. Robert W. Wood discovered an unexplained phenomenon that on many diffraction gratings narrow spectral regions showed a sharp change of energy diffracted. In his work, he said “I was astounded to find that under certain conditions, the drop from maximum illumination to minimum occurred within a range of wavelengths not greater than the distance between the sodium lines” [5]. The main point of Wood’s discovery was that these lines were present only when the magnetic field is parallel to the grating grooves (this light is p -polarized, see Chapter 2.2), although he was unable to provide any interpretation to these phenomena [6].

By the year 1904, Maxwell Garnett studied the bright colors observed in metal-doped glasses [7] and described the effect examined on Lycurgus cup using newly developed Drude theory of metals (see Chapter 2.4) and the electromagnetic properties of small spheres as derived by Lord Rayleigh. He developed a theory of effective dielectric constant - the Maxwell-Garnett theory. Garnett’s work was extended by Gustav Mie in 1908 who develops theory of light scattering by spherical particles [8]. The solution of Maxwell’s equations that had a “surface wave” property was

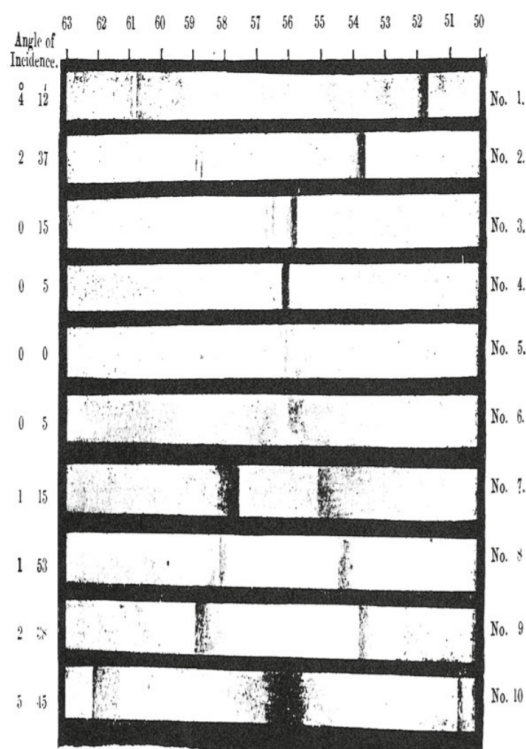


Figure 1.2: Spectra of a continuous light source obtained by Wood for some values of the angle of incidence. The wavelength in nanometers is obtained by multiplying by factor of 10 to the numbers shown at the top of the figure. On the left are shown angles of incidence. On No.1 the narrow line appeared in the yellow ($\lambda \approx 610$ nm), while the larger dark line was observed in the green ($\lambda \approx 520$ nm). Decreasing the angle of incidence, these lines approached one another, and at normal incidence, the lines brought together and a uniform illumination was observed. Then, with an incidence on the other side of the normal, lines separated again. These lines were extremely bright up to a certain wavelength where the intensity very suddenly dropped to values close to zero, this fall occurring within a range not greater than the distance between the sodium lines [4].

analyzed in 1907 by Jonathan Zenneck. Surface plasmon was theoretically described fifty years later in 1957 in the study by Rufus Ritchie [9] on electron energy losses in thin films and nearly seventy years after Wood's original observations, Rufus Ritchie described anomalous phenomena of metal gratings regarding surface plasmons resonances excited on gratings [10]. In 1968 Andreas Otto and Erich Kretschmann with Heinz Raether presented first methods for optical excitation of surface plasmons on metal films [11, 12].

Since then, the field of plasmonics (the science and technology of metal-based optics and nanophotonics) have experienced quick development which is clearly reflected in the scientific literature as is shown in Figure 1.3. The surface plasmon

has unique properties and may overcome current technologies that are approaching fundamental physical limits. For researchers in the field of optics, one of the most attractive aspects of surface plasmons is the way in which they help us to concentrate and channel light using sub-wavelength structures. Concentrated light can be used to manipulate light-matter interactions and boost non-linear phenomena. A wide range of plasmon-based optical elements and techniques have been developed – we can fabricate extremely compact plasmonics waveguide structures, couplers, active switches, lithographic masks and so on. For example, a technique called surface-enhanced Raman spectroscopy (SERS) can detect a single molecule and is based on metallic structures much smaller than the wavelength of light that are vital for massive signal enhancement [13].

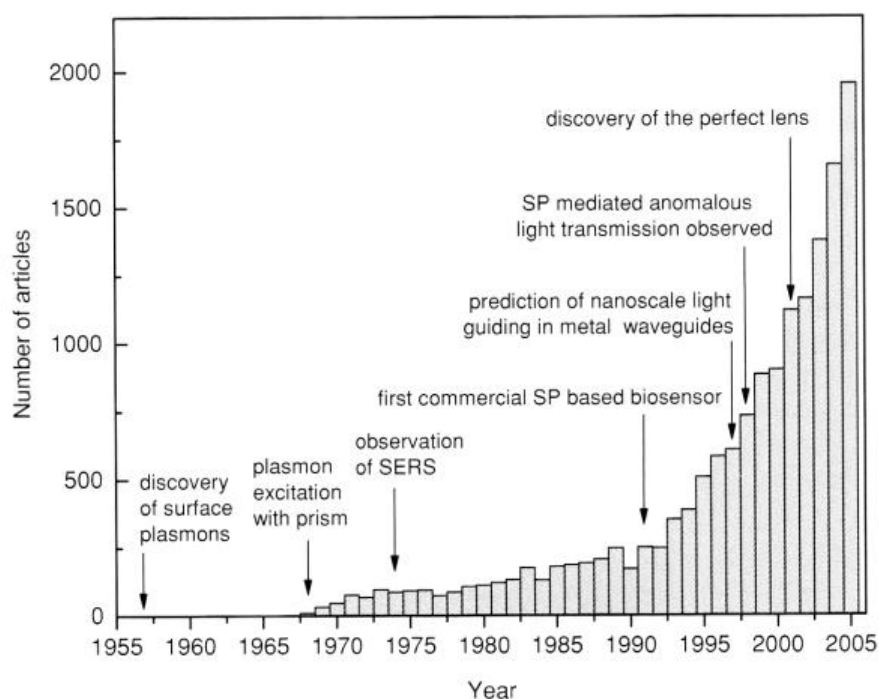


Figure 1.3: The number of scientific articles published from 1955 to 2005 containing the phrase “surface plasmon” in either the title or abstract illustrates the growth of the field of metal nanophotonics. Since 1990 the annual number of publications has been increasing almost exponentially [6].

Another well-known plasmonic effect, called surface plasmon resonance (SPR), is widely used in various physical, chemical and biological applications, mostly in very sensitive detectors [3]. At present, an estimated 50% of all publications on surface plasmons involve the use of plasmons for biodetectors [6]. SPR method is very powerful tool for many types of interference studies and is excellent for monitoring

changes of the refractive index in the near vicinity of the metal surface, and it is suited to measure the difference between two states and also to monitor the change in time. These sensors investigate a very limited vicinity or fixed volume at the metal surface. They use only evanescent field with low penetration depth at which a signal is observed (not more than few hundred nanometers), decaying exponentially with the distance from the metal layer at the sensor surface [3].

The growth of plasmonics is also based on the development of bottom-up and top-down techniques for fabricating metallic nanostructures, such as electron-beam lithography [14], focused ion beam milling [15] and various chemical synthesis methods [16]. Recent development of relatively cheap numerical simulations tools helps to visualize the electromagnetic fields on metallic nanostructures and to develop new ones.

One of the advanced topics of plasmonics is the use of the magneto-optics at terahertz range for adjustment of the signal. Materials exhibiting a magneto-optical (MO) behavior at this range are for example graphene[17], hexaferrites [18] and semiconductors [19, 17]. We discuss the use of magneto-optics for surface plasmon resonance and waveguide structures in Chapter 4.2 and 5.2.

1.1 Organization of the thesis

The thesis contains six chapters divided into four major topics which are indicated below.

The first chapter contains brief history, trends and applications of plasmonics.

Chapter 2 reviews the theoretical foundations of the electromagnetics, the first part of this chapter provides an analysis of Maxwell's equations and is followed by analysis of a reflection and refraction of a plane electromagnetic wave at the single interface and the thin film. In the second part, a qualitative introduction to the fundamentals of surface plasmons is given. At last, the model describing material properties are investigated.

Chapter 3 demonstrates the benefits of numerical methods, especially Finite elements method which is a headstone of COMSOL Multiphysics software. The basic numeric model of the rectangular waveguide is illustrated and, in the latter part of the chapter, the main steps in modeling with COMSOL Multiphysics are summarized.

In Chapter 4 models of structures used for excitation of plasmons are shown. Reflectance as a function of variable parameters in Kretschmann-Raether and Otto configuration is computed by COMSOL Multiphysics and compared with analytical results. The Otto configuration with the external magnetic field is discussed compared with the experiment.

Basic surface plasmon waveguide models created with COMSOL Multiphysics are presented in Chapter 5. The application of external magnetic field on the metal cylinder waveguide is investigated.

Finally, Chapter 6 summarizes and concludes the thesis.

2 Electromagnetics Background

2.1 Maxwell's equations

The Maxwell equations are very well known. They are presented in one of two forms, differential or integral. We will use the differential form. The first - Faraday's law of electromagnetic induction - states that the curl of the electric field vector \mathbf{E} is proportional to the time derivative of the magnetic flux density vector \mathbf{B}

$$\nabla \times \mathbf{E} = -\frac{\partial \mathbf{B}}{\partial t}. \quad (2.1)$$

The second equation is based on Ampere's circuit law and it relates a spatial derivative of the magnetic field strength \mathbf{H} to the time derivative of the electric displacement vector \mathbf{D}

$$\nabla \times \mathbf{H} = \mathbf{J} + \frac{\partial \mathbf{D}}{\partial t}. \quad (2.2)$$

We assume that source-current density $\mathbf{J} = 0$, so we can write

$$\nabla \times \mathbf{H} = \frac{\partial \mathbf{D}}{\partial t}. \quad (2.3)$$

Next two equations are attributed to Gauss. First of them called the law of electrostatic relates the divergence of the electric displacement vector to the charge density

$$\nabla \mathbf{D} = \rho, \quad (2.4)$$

and because we assume the charge density is zero we can write this equation in the form

$$\nabla \mathbf{D} = 0. \quad (2.5)$$

The last Maxwell's equation is called Gauss's law for magnetic fields and relates the divergence of the magnetic flux density to the density of the magnetic monopoles. Because these monopoles do not exist we write

$$\nabla \mathbf{B} = 0. \quad (2.6)$$

Two electric vectors (\mathbf{D} and \mathbf{E}) with two magnetic vectors (\mathbf{B} and \mathbf{H}) can be connected by constitutive relations, so we can separate the contributions to \mathbf{B} and \mathbf{D} into free-space parts and parts related to the material properties [20]

$$\mathbf{D} = \varepsilon \mathbf{E} = \varepsilon_0 \mathbf{E} + \mathbf{P}, \quad (2.7)$$

$$\mathbf{B} = \mu \mathbf{H} = \mu_0 \mathbf{H} + \mathbf{M}, \quad (2.8)$$

where $\varepsilon = \varepsilon_0 \varepsilon_r$ is the permittivity of medium, $\varepsilon_0 = 8.8542 \cdot 10^{-12} Fm^{-1}$ is the permittivity of vacuum, \mathbf{P} is the vector of polarization, $\mu = \mu_0 \mu_r$ is the permeability of medium, $\mu_0 = 4\pi \cdot 10^{-7} Hm^{-1}$ is the permeability of vacuum and \mathbf{M} is the vector of magnetization. We also may define the electric susceptibility χ_e and the magnetic susceptibility χ_m

$$\mathbf{D} = \varepsilon_0 \varepsilon_r \mathbf{E} = \varepsilon_0 (1 + \chi_e) \mathbf{E}, \quad (2.9)$$

$$\mathbf{B} = \mu_0 \mu_r \mathbf{H} = \mu_0 (1 + \chi_m) \mathbf{H}. \quad (2.10)$$

We write the boundary conditions of Maxwell's equation on interface of two media in case of $\rho = 0$ and $\mathbf{J} = 0$ in the form

$$\mathbf{n} \cdot (\mathbf{D}_{1n} - \mathbf{D}_{2n}) = 0, \quad (2.11a)$$

$$\mathbf{n} \cdot (\mathbf{B}_{1n} - \mathbf{B}_{2n}) = 0, \quad (2.11b)$$

$$\mathbf{n} \times (\mathbf{E}_{1t} - \mathbf{E}_{2t}) = 0, \quad (2.11c)$$

$$\mathbf{n} \times (\mathbf{H}_{1t} - \mathbf{H}_{2t}) = 0. \quad (2.11d)$$

In our case, we consider absence of current densities and nonmagnetic materials $\mu_r = 1$. The Maxwell's equations (2.1) and (2.3) can be combined, as

$$\nabla \times \nabla \times \mathbf{E} = -\mu_0 \frac{\partial^2 \mathbf{D}}{\partial t^2} \quad (2.12)$$

$$\nabla(\nabla \cdot \mathbf{E}) - \nabla^2 \mathbf{E} = -\mu_0 \varepsilon \frac{\partial^2 \mathbf{E}}{\partial t^2}. \quad (2.13)$$

Because there are no external charges, we get

$$\nabla\left(-\frac{1}{\varepsilon} \nabla \varepsilon\right) - \nabla^2 \mathbf{E} = -\frac{\varepsilon_r}{c^2} \frac{\partial^2 \mathbf{E}}{\partial t^2}, \quad (2.14)$$

where $c = \frac{1}{\sqrt{\varepsilon_0 \mu_0}}$ is the speed of light in free space. The variation of the dielectric profile $\varepsilon = \varepsilon(\mathbf{r})$ over distances on the order of one optical wavelength is negligible.

In general, for assuming a harmonic time dependence of the electric field, we can write

$$\nabla^2[\mathbf{E}(\mathbf{r})e^{i\omega t}] - \frac{\varepsilon}{c^2} \frac{\partial^2[\mathbf{E}(\mathbf{r})e^{i\omega t}]}{\partial t^2} = 0, \quad (2.15)$$

so we obtain the time-independent form of the wave equation which is known as Helmholtz equation

$$\nabla^2\mathbf{E} + k_0^2\varepsilon_r\mathbf{E} = 0, \quad (2.16)$$

where $k_0 = \frac{\omega}{c} = \frac{2\pi\nu}{c} = \frac{2\pi}{\lambda}$ is referred to as the wavenumber of the propagating wave in the free space, $\lambda = \frac{c}{\nu}$ as the wavelength and ν as a frequency.

2.2 Reflection of a plane wave and polarization modes

Solutions of Maxwell's equations can be classified into two orthogonal linear polarization modes, which are referred to as transverse magnetic and transverse electric mode. Transverse magnetic (TM) since the magnetic field is orthogonal to the plane of incidence, or the parallel polarization (*p-polarization*) since the electric field is parallel to the plane of incidence. Transverse electric (TE) because the electric field is orthogonal to the plane of incidence. TE mode is also called *s-polarization* from the German *senkrecht* which means perpendicular.

When a plane wave from one medium meets a different medium it can be reflected or transmitted or both. A transmitted wave proceeds into the second medium and a reflected wave propagates back into the first medium. The proportion depends on the constitutive parameters which were mentioned before. Uniform incident plane wave takes the general form of

$$\mathbf{E}_i = \mathbf{E}_{0,i}e^{i(\mathbf{k}_i\mathbf{r}-\omega_i t)}, \quad (2.17)$$

where $\mathbf{k}_i = \mathbf{k}_{xi} + \mathbf{k}_{yi} + \mathbf{k}_{zi}$ is the propagation vector (or wave vector) as is depicted in Figure 2.1 and is always in the direction of wave propagation and $\mathbf{r} = \mathbf{x} + \mathbf{y} + \mathbf{z}$ is the position vector [21]. The magnitude of the propagation vector is tightly related to the frequency of wave ω by dispersion relation

$$k_i^2 = k_{ix}^2 + k_{iy}^2 + k_{iz}^2 = \omega^2\mu\varepsilon \quad (2.18)$$

Maxwell's equations for source-free region for the plane wave can be expressed as

$$\mathbf{k} \times \mathbf{E} = \omega\mu\mathbf{H}, \quad (2.19a)$$

$$\mathbf{k} \times \mathbf{H} = -\omega\varepsilon\mathbf{E}, \quad (2.19b)$$

$$\mathbf{k} \cdot \mathbf{E} = 0, \quad (2.19c)$$

$$\mathbf{k} \cdot \mathbf{H} = 0. \quad (2.19d)$$

The scalar product shows that \mathbf{E} , \mathbf{H} and \mathbf{k} are perpendicular to each other. The electric field vector \mathbf{E} and the vector of the magnetic field strength \mathbf{H} lie on the plane $\mathbf{k}\mathbf{r} = \text{constant}$. The plane defined by the propagation vector \mathbf{k} and a unit normal vector \mathbf{n} to the boundary is called the plane of incidence. The angle between \mathbf{k} and \mathbf{n} is the angle of incidence. We write the incidence, the reflected and the transmitted wave as

$$\mathbf{E}_i = \mathbf{E}_{0,i} e^{i(k_{ix} + k_{iy} + k_{iz} - \omega_i t)}, \quad (2.20a)$$

$$\mathbf{E}_r = \mathbf{E}_{0,r} e^{i(k_{rx} + k_{ry} + k_{rz} - \omega_r t)}, \quad (2.20b)$$

$$\mathbf{E}_t = \mathbf{E}_{0,t} e^{i(k_{tx} + k_{ty} + k_{tz} - \omega_t t)}. \quad (2.20c)$$

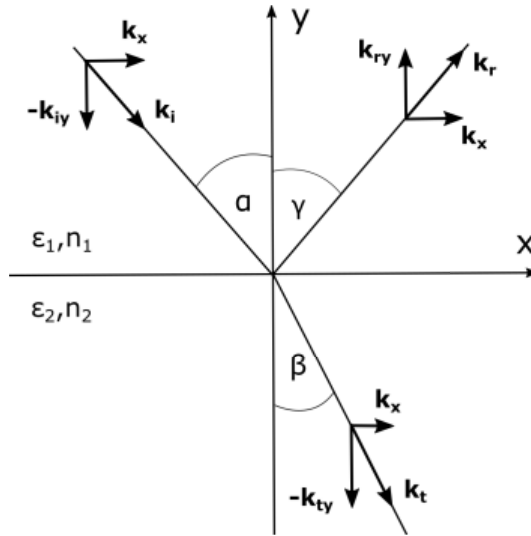


Figure 2.1: Reflection and refraction at a planar optical interface between two semi-infinite media.

The tangential component of \mathbf{E} must be continuous as well as tangential components of propagation vectors which imply that the frequency of the incident, the reflected and the transmitted wave is unchanged ($\omega_i = \omega_r = \omega_t = \omega$) and vectors \mathbf{k}_i ,

\mathbf{k}_r and \mathbf{k}_t lie in the plane of incidence, so we can derive from these conditions

$$k_i \sin \alpha = k_r \sin \gamma, \quad (2.21)$$

$$k_i \sin \alpha = k_t \sin \beta, \quad (2.22)$$

where α , β and γ angles of incidence, transmission, and reflection. We shall write: $k_i = k_r = 2\pi\omega n_1$ and $k_t = 2\pi\omega n_2$, where n_1 and n_2 are refractive indexes of the media and we easily obtain the law of reflection

$$\alpha = \gamma, \quad (2.23)$$

as well as Snell's law of refraction

$$n_1 \sin \alpha = n_2 \sin \beta. \quad (2.24)$$

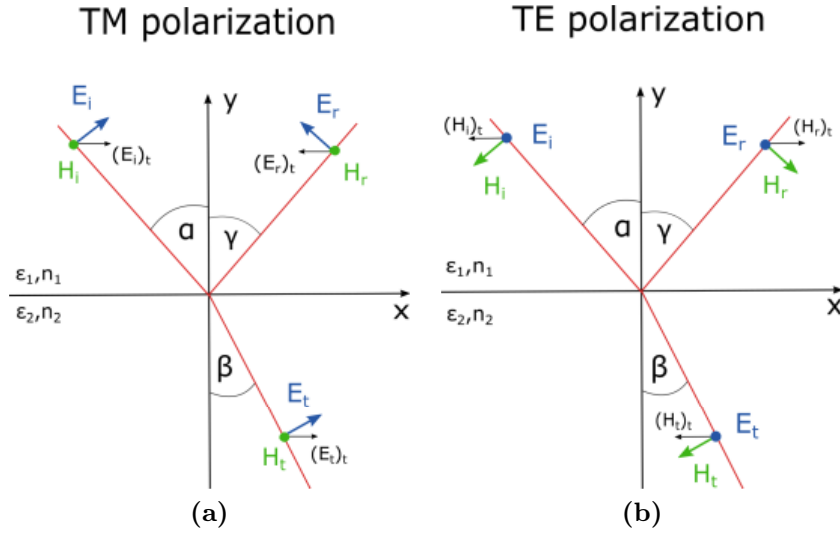


Figure 2.2: Reflection and refraction for TM and TE polarization (p - and s -polarization) at the planar optical interface. Electric field, magnetic field and their tangential components are depicted [22].

The electric field on incident light can be decomposed into orthogonal and linearly polarized waves with parallel (\mathbf{E}_p) and perpendicular (\mathbf{E}_s) components with respect to the plane of incidence. From amplitude comparison $(E_i)_{tang.} + (E_r)_{tang.} = (E_t)_{tang.}$, $(H_i)_{tang.} + (H_r)_{tang.} = (H_t)_{tang.}$. Fresnel coefficients can be derived:

$$r_s = \frac{E_{s,r}}{E_{s,i}} = \frac{n_1 \cos \alpha - n_2 \cos \beta}{n_1 \cos \alpha + n_2 \cos \beta}, \quad (2.25a)$$

$$r_p = \frac{E_{p,r}}{E_{p,i}} = \frac{n_2 \cos \alpha - n_1 \cos \beta}{n_2 \cos \alpha + n_1 \cos \beta}, \quad (2.25b)$$

$$t_s = \frac{E_{s,t}}{E_{s,i}} = \frac{2n_1 \cos \alpha}{n_1 \cos \alpha + n_2 \cos \beta} = 1 + r_s, \quad (2.25c)$$

$$t_p = \frac{E_{p,t}}{E_{p,i}} = \frac{2n_1 \cos \alpha}{n_2 \cos \alpha + n_1 \cos \beta} = \frac{n_1}{n_2} (1 + r_p), \quad (2.25d)$$

where r_s and r_p are forward reflection coefficients for s - and p - polarization and t_s and t_p are forward transmission coefficients for s - and p - polarization. The transmission coefficient measures how much of the electromagnetic wave passes through an optical element while the reflection coefficient describes how much of the wave is reflected. From symmetries we can define backward coefficients for electromagnetic waves traveling in the reverse direction

$$\tilde{r}_s = -r_s, \quad (2.26a)$$

$$\tilde{r}_p = -r_p, \quad (2.26b)$$

$$\tilde{t}_s = 1 - r_s, \quad (2.26c)$$

$$\tilde{t}_p = \frac{n_2}{n_1} (1 - r_p), \quad (2.26d)$$

where $t_{s,p} \tilde{t}_{s,p} - r_{s,p} \tilde{r}_{s,p} = 1$. The fraction of the incident electromagnetic power that is reflected or transmitted at an interface is called reflectance or transmittance respectively. For both s - and p - polarization the reflectance is defined as

$$R_{s,p} = \left| \frac{\mathbf{E}_r}{\mathbf{E}_i} \right|_{s,p}^2 = |r_{s,p}|^2 \quad (2.27)$$

and the transmittance is defined as

$$T_{s,p} = \frac{n_2 \cos \beta}{n_1 \cos \alpha} |t_{s,p}|^2. \quad (2.28)$$

Thin-film interference

The presence of two optical interfaces, each with characteristic Fresnel coefficients for reflection and transmission, leads to division of the incident beam into a multitude of coherent waves as shown in the Figure 2.3. The superposition of these coherent

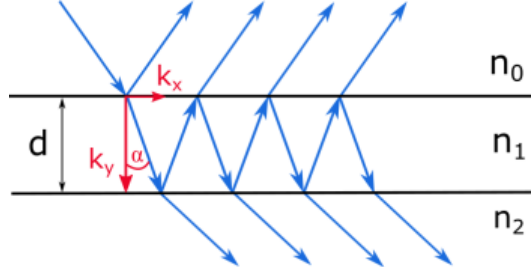


Figure 2.3: Reflection and transmission on a thin film [22].

waves results in the interference. Higher order reflected waves contribute to the result which is dependent on the thickness of the film and refractive indexes of media. The resultant amplitude is equal to the vector sum of the individual amplitudes, so we distinguish the constructive and the destructive interference. The constructive (or destructive) interference occurs when the phase difference between the waves is an even (or an odd) multiple of π . Propagation in thin film is given by $e^{ik_y d} = e^{ik_0 n_1 \cos \alpha d}$, where $k_y = 2\pi\omega n_1 \cos \alpha$.

For partial reflected wave applies Fresnel formula $r_{s,p}^{(01)}$ and for partial transmitted wave applies $t_{s,p}^{(01)} t_{s,p}^{(12)} e^{ik_y d}$. With use of geometric series we can write the transmission coefficient as

$$t_{s,p}^{(012)} = \frac{t_{s,p}^{(01)} t_{s,p}^{(12)} e^{ik_y d}}{1 - r_{s,p}^{(01)} \tilde{r}_{s,p}^{(12)} e^{i2k_y d}} = \frac{t_{s,p}^{(01)} t_{s,p}^{(12)} e^{ik_y d}}{1 + r_{s,p}^{(01)} r_{s,p}^{(12)} e^{i2k_y d}}. \quad (2.29)$$

The reflection coefficient can be obtained analogically

$$r_{s,p}^{(012)} = r_{s,p}^{(01)} + \frac{t_{s,p}^{(01)} r_{s,p}^{(12)} \tilde{r}_{s,p}^{(10)} e^{i2k_y d}}{1 - \tilde{r}_{s,p}^{(10)} r_{s,p}^{(12)} e^{i2k_y d}} = \frac{r_{s,p}^{(01)} + r_{s,p}^{(12)} e^{i2k_y d}}{1 + r_{s,p}^{(01)} r_{s,p}^{(12)} e^{i2k_y d}}. \quad (2.30)$$

2.3 Fundamentals of surface plasmons

We consider a classical model consisting of two semi-infinite nonmagnetic media with local frequency-dependent dielectric functions ε_1 and ε_2 separated by a planar interface at $y = 0$ and p -polarized electromagnetic wave. For an ideal isotropic, non-magnetic surface, waves propagating along interface must necessarily have a component of electric field normal to the surface, so s -polarized surface oscillations do not exist [3].

Choosing the x -axis along the propagating direction, we can set amplitudes of the components of the magnetic field \mathbf{H} and electric field \mathbf{E}

$$H_j = (0, 0, H_{zj}), \quad (2.31)$$

$$E_j = (E_{xj}, E_{yj}, 0), \quad (2.32)$$

and we shall write

$$\mathbf{H}_j = (0, 0, H_{zj})e^{i(k_{xj}x+k_{yj}y-\omega t)}, \quad (2.33)$$

$$\mathbf{E}_j = (E_{xj}, E_{yj}, 0)e^{i(k_{xj}x+k_{yj}y-\omega t)}. \quad (2.34)$$

Introducing these equations into equation (2.3) with use of constitutive relations (2.9) and (2.10), we obtain

$$\nabla \times \mathbf{H} = \varepsilon \frac{\partial \mathbf{E}}{\partial t}, \quad (2.35)$$

so

$$-H_{zj}k_{xj} = \varepsilon_j E_{yj}\omega, \quad (2.36)$$

$$H_{zj}k_{zj} = \varepsilon_j E_{xj}\omega, \quad (2.37)$$

where $j = 1$ or 2 . The boundary conditions (2.11) imply that the component of the electric and magnetic fields parallel to the surface must be continuous. Tangential components $H_{z1} = H_{z2} \equiv H_z$, $E_{x1} = E_{x2} \equiv E_x$ and normal component $\varepsilon_1 E_{y1} = \varepsilon_2 E_{y2}$ have to be conserved, so we obtain from (2.36)

$$-H_z k_{x1} = \varepsilon_1 E_{y1}\omega, \quad (2.38)$$

$$-H_z k_{x2} = \varepsilon_1 E_{y1}\omega, \quad (2.39)$$

and we get interface condition

$$k_{x1} = k_{x2} \equiv k_x. \quad (2.40)$$

From equation (2.37) together with the continuity relations follows

$$H_z k_{y1} = \varepsilon_1 E_{x1}\omega, \quad (2.41)$$

$$H_z k_{y2} = \varepsilon_2 E_{x1}\omega, \quad (2.42)$$

so

$$\frac{k_{y1}}{\varepsilon_1} = \frac{k_{y2}}{\varepsilon_2}, \quad (2.43)$$

which is the condition of the surface plasmon and we obtain the equation of the wave number

$$k_j^2 = \varepsilon_j \frac{\omega^2}{c^2} = k_x^2 + k_{yj}^2. \quad (2.44)$$

From Figure 2.1 we can set components $k_{x1} = k_1 \sin \alpha = \sqrt{\varepsilon_1} \frac{\omega}{c} \sin \alpha$, $k_{y2} = \sqrt{k_2^2 - k_{x2}^2} = \sqrt{\varepsilon_2 k_0^2 - k_x^2}$ and $k_{y1} = \sqrt{\varepsilon_1 k_0^2 - k_x^2}$ and introduce them to the equation (2.43)

$$\frac{\sqrt{\varepsilon_1 k_0^2 - k_x^2}}{\varepsilon_1} = \frac{\sqrt{\varepsilon_2 k_0^2 - k_x^2}}{\varepsilon_2}. \quad (2.45)$$

Hence, we obtain the expression for propagating constant of surface plasmon wave

$$k_x = \beta = \frac{\omega}{c} \sqrt{\frac{\varepsilon_1 \varepsilon_2}{\varepsilon_1 + \varepsilon_2}}. \quad (2.46)$$

Similarly, using (2.43), we get expression for component k_{yj}

$$k_{yj} = \frac{\omega}{c} \sqrt{\frac{\varepsilon_j^2}{\varepsilon_1 + \varepsilon_2}}, \quad (2.47)$$

where $\frac{\omega}{c} = k_0$ represents the magnitude of the light wave vector and β_{SP} is the propagation constant of a surface plasma wave. These equations are the sought SPR dispersion equation (see Figure 2.4) for an interface between two half-infinite media. We assume ω and ε_2 is real, β is complex because the permittivity is complex $\varepsilon_1 = \varepsilon_1' + i\varepsilon_1''$ (for more information about the permittivity see Chapter 2.4).

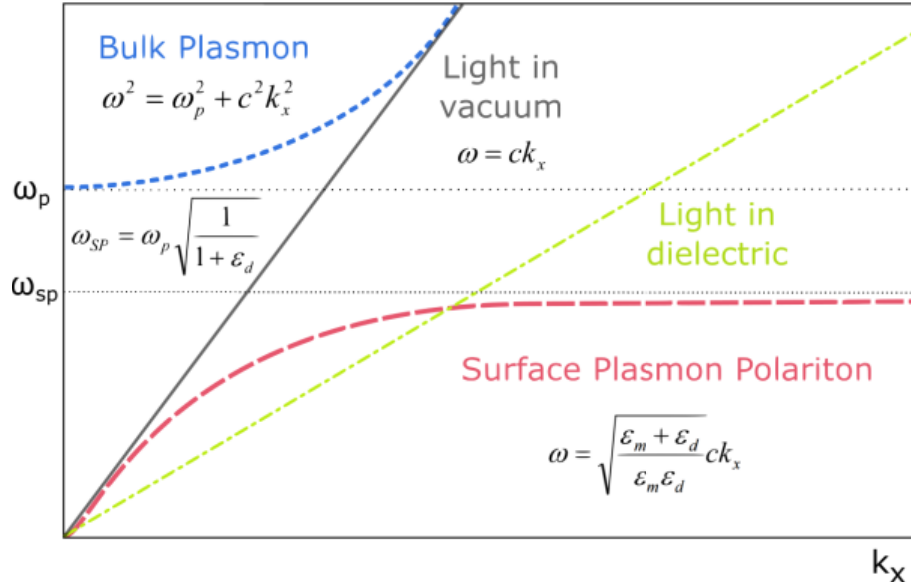


Figure 2.4: The dispersion relation for bulk plasmons, free-space electromagnetic waves, electromagnetic waves in dielectric and surface plasmons. The permittivity of the dielectric is denoted as ε_d , the permittivity of the metal as ε_m and ω_p is plasma frequency (see Chapter 2.4).

As the surface plasmon propagates along the surface, its intensity sharply decays. We define the propagation distance as the distance for the surface plasmon intensity to decay to $1/e$ of its original value,

$$L_p = \frac{1}{2\Im(k_x)}, \quad (2.48)$$

where k_x is the propagation constant. Likewise, the electric field falls off evanescently perpendicular to the metal surface, but in the dielectric the field decays far more slowly.

Sometimes is useful to define ν_x as k_x/k_0

$$\nu_x = \sqrt{\frac{\varepsilon'_1 \varepsilon_2}{\varepsilon'_1 + \varepsilon_2}}, \quad (2.49)$$

If we assume that ν_x is real, the expression under the square root has to be non-negative number

$$\frac{\varepsilon'_1 \varepsilon_2}{\varepsilon'_1 + \varepsilon_2} > 0, \quad (2.50)$$

so for real ν_x and one needs $\varepsilon'_1 < 0$ and $|\varepsilon'_1| > \varepsilon_2$, which can be fulfilled in a metal and also in a doped semiconductor below plasma frequency. Metals such as gold, silver and aluminum exhibit considerable imaginary parts of the permittivity, which causes the propagation constant of a surface plasmon to have a non-zero imaginary part that is associated with the attenuation of the surface plasmon in the direction of propagation. The field perpendicular to the surface decays exponentially with distance from the surface and is said to be evanescent field. It is consequence of the bound, non-radiative nature of SPs, which prevents power from propagating away from the surface [23].

2.4 Material properties

Lorentz oscillator

Maxwell's equations are great way how to describe electromagnetic field, but they provide no insight into the mechanism of the interaction of light with matter in the optical domain which occurs primarily with electrons.

In 1895 Hendrik A. Lorentz introduced a model of an electron as a mass on a set of springs [24]. This model is designed for insulators, or, at least for electrons

which are bound by some force to an atom or ion in the solid and can be applied to lattice vibration in compound crystals. Localized electrons in atoms are considered as classic oscillators.

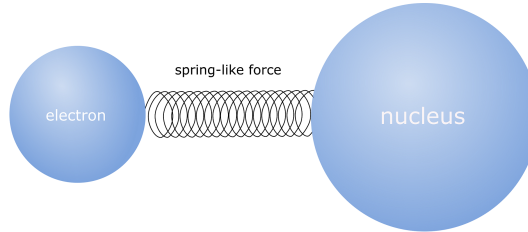


Figure 2.5: Lorentz oscillator. Electrons are considered as charged masses attached to springs.

The dipole moment is generated between an electron with negative charge and the nucleus of atom with positive charge when the electron is shifted from equilibrium position and spring provide a restoring force that returns the electron to it. The solid is considered as a group of independent harmonic oscillators. We will view the potential for these bound electrons as harmonic and the spring constant will be the same for all the electrons in a particular orbital.

The equation of the motion of localized electrons in one dimension x is

$$F = m_e a = m_e \frac{d^2 x}{dt^2}, \quad (2.51)$$

where $m_e = 9.11 \cdot 10^{-31} kg$ denotes the electron mass and F is the force acting on the electron. We can set

$$F = -eE - \kappa x - \Gamma v. \quad (2.52)$$

E in the first term represents the external oscillating electric force acting on the electron of the charge e : $E = E_0 e^{i\omega t}$. The molecule has zero dipole moment without an external field.

The second term is attracting harmonic force of atomic core, which is proportional to deviation x (with respect to the equilibrium) and the “spring” constant $\kappa = m_e \omega_L^2$, where ω_L is the oscillator resonant frequency. The electron is considered to be bound to the zero position by this force.

The third term denotes damping force which is proportional to the velocity where Γ is the damping constant and $v = \frac{dx}{dt}$. Now, we can easily obtain the equation of motion of localized electrons

$$-eE_0 e^{i\omega t} = m_e \frac{d^2 x}{dt^2} + \Gamma \frac{dx}{dt} + m_e \omega_L^2 x. \quad (2.53)$$

We expect the solution of this equation in the form $x = x_0 e^{i\omega t}$. Taking the first derivate and the second derivate, equation (2.53) for displacement x_0 becomes

$$x_0 = -\frac{eE_0}{m_e(\omega_L^2 - \omega^2) - i\Gamma\omega}. \quad (2.54)$$

With this displacement, the dipole moment is $p = -ex_0$ and the polarization is

$$P = Np = \frac{e^2 N}{m_e} \frac{E_0}{\omega_L^2 - \omega^2 - i\frac{\Gamma}{m_e}\omega}, \quad (2.55)$$

where N denotes a number of dipole moments of electrons (charged particles). The electric susceptibility $\chi_e = \frac{pN}{\epsilon_0 E}$ can be expressed in the form

$$\chi_e = \frac{\frac{e^2 N}{\epsilon_0 m_e}}{\frac{\kappa}{m_e} - \omega^2 - i\omega\frac{\Gamma}{m_e}} = \frac{A_L \omega_L^2}{\omega_L^2 - \omega^2 - i\omega\gamma_L}, \quad (2.56)$$

where $A = \frac{e^2 N}{\epsilon_0 m_e} = A_L \omega_L^2$, A_L is the oscillator amplitude, $\omega_L^2 = \frac{\kappa}{m_e}$ is the oscillator resonant frequency and $\gamma_L = \frac{\Gamma}{m_e}$ is the oscillator damping [25, 26].

Drude model for free electrons

In metals, conductive electrons are not strictly localized; they can move in whole conduction band. In n-type semiconductors, free electrons are in conductive band. We assume that all atoms contribute to electron gas by the same number of electrons, electron gas is ideal gas with Maxwell-Boltzmann distribution of velocities and electrons are free and independent. We come out from equation of force

$$F = m_e a = m_e \frac{d^2 x}{dt^2}, \quad (2.57)$$

where $m_e = 9.109 \cdot 10^{-31} \text{kg}$ is the mass of electron and force F denotes effect of Coulomb field on the charge, so we shall write

$$F = -eE - \Gamma v. \quad (2.58)$$

$e = 1.602 \cdot 10^{-19} \text{C}$ is charge of the electron, γ is the decay constant and $v = \frac{dx}{dt}$ is the electron speed. The first term of equation represents monochromatic electric force $E = E_0 e^{i\omega t}$ acting on electron and second term is decaying force. From equations

(2.57) and (2.58) we obtain kinetic equation of motion of free electrons easily

$$m_e \frac{d^2x}{dt^2} + \Gamma \frac{dx}{dt} = -eE_0 e^{i\omega t}. \quad (2.59)$$

The solution of this equation is expected in the form $x = x_0 e^{i\omega t}$, so we can simply express x_0

$$x_0 = \frac{-eE_0}{m_e \omega^2 - i\Gamma\omega}. \quad (2.60)$$

Dipole moment can be also obtained from the displacement of electron

$$p = -ex_0. \quad (2.61)$$

Polarization is volume density of dipole moments, so we can write

$$P = Np = \frac{Ne^2 E_0}{m_e(\omega^2 - i\frac{\Gamma}{m_e}\omega)}, \quad (2.62)$$

where N is carrier concentration. The equation of polarization is used for the expression of electric susceptibility χ_e , because

$$\chi_e = \frac{P}{\varepsilon_0 E}. \quad (2.63)$$

Relative permittivity is associated with the electric susceptibility

$$\varepsilon_r = \varepsilon_\infty + \chi_e = \varepsilon_\infty + \frac{e^2 N}{m_e \varepsilon_0} \frac{1}{\omega^2 - i\frac{\Gamma\omega}{m_e}} = \varepsilon_\infty + \frac{\omega_p^2}{\omega^2 - i\gamma_D \omega}, \quad (2.64)$$

where $\omega_p = \sqrt{\frac{e^2 N}{m_e \varepsilon_0}}$ is the plasma frequency, $\gamma_D = \frac{\Gamma}{m_e}$ is the damping term, ε_∞ is the high frequency permittivity and $m_e = m_{\text{eff}} m_0$ is effective mass of charge carriers (m_0 is the mass of electron in vacuum). Plasma frequency corresponds to the frequency of oscillations of electron gas with given density N [27].

Thus, the Drude dielectric function is given by

$$\varepsilon_r = \varepsilon_\infty + \frac{\omega_p^2}{\omega(\omega - i\gamma)}. \quad (2.65)$$

Since the electric permittivity is a complex quantity, we can separate a real and an imaginary part

$$\varepsilon_r = \varepsilon_\infty + \frac{\omega_p^2}{\omega^2 + \gamma_D^2} + i \frac{\omega_p^2 \gamma_D}{\omega(\omega^2 + \gamma_D^2)}. \quad (2.66)$$

The Drude model is elementary classical treatment of optical properties of metals but it is also used for semiconductors which behave similarly to simple metals (sufficiently doped).

Drude-Lorentz model

For cases where we can use nor Drude model of free electron conductivity neither Lorentz model of dipole oscillators we use Drude-Lorentz model which combines both and describes the dielectric function of semiconductors in the frequency range properly. The proposed dielectric function is given by

$$\varepsilon_r = \varepsilon_\infty - \frac{\omega_p^2}{\omega(\omega - i\gamma)} + \frac{A\omega_L^2}{\omega_L^2 - \omega^2 - i\omega\gamma_L}, \quad (2.67)$$

where the first term describes high frequency permittivity (background permittivity), the second term is the Drude term and the last term is the Lorentz term.

Permittivity

The permittivity is a constant of proportionality between electric displacement \mathbf{D} and electric field density \mathbf{E} (see Equation (2.7)). The isotropic materials with the same optical properties in all directions can be easily described by complex permittivity $\varepsilon = \varepsilon' + i\varepsilon''$, where ε' is the real part and ε'' is the imaginary part as shows the Figure 2.6. The imaginary part describes the loss in the material so for lossless materials we can write only the real part.

Anisotropic materials have not the same optical properties in all directions and their \mathbf{D} , \mathbf{E} and \mathbf{P} are not parallel, so the permittivity has to be expressed as a tensor $\hat{\varepsilon}$ with nine components

$$\hat{\varepsilon} = \underbrace{\begin{bmatrix} \varepsilon_{xx} & \varepsilon_{xy} & \varepsilon_{xz} \\ \varepsilon_{yx} & \varepsilon_{yy} & \varepsilon_{yz} \\ \varepsilon_{zx} & \varepsilon_{zy} & \varepsilon_{zz} \end{bmatrix}}_{\hat{\varepsilon}_r} \cdot \varepsilon_0, \quad (2.68)$$

where $\hat{\varepsilon}_r$ is the relative permittivity tensor and ε_0 is the permittivity of free space ($\varepsilon_0 = 8.854 \cdot 10^{-12} F/m$) [21].

The optical anisotropy can be achieved in several ways, e.g. in anisotropic crystals is caused by the character of their structure. These crystals exhibit properties

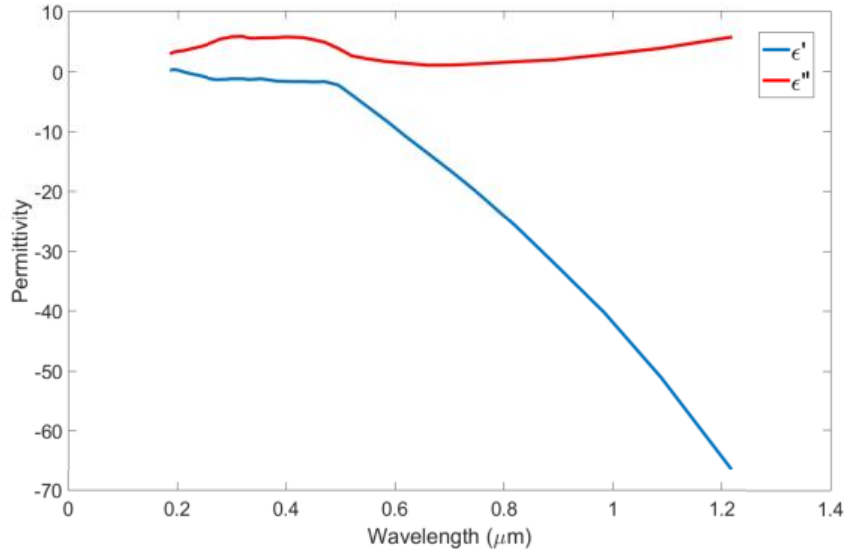


Figure 2.6: Experimental data of permittivity of a gold obtained by *Johnson and Christy* [28].

such as birefringence which means that their refractive index depends on the polarization and propagation direction of the electromagnetic wave.

In this thesis we discuss the optical anisotropy caused by applying external magnetic field (Chapter 4.2) according to the experiments by *Chochol et al.* [29].

We apply magnetic flux density B in transversal direction, so the permittivity tensor changes with respect to the direction to:

- \mathbf{B}_x :

$$\hat{\epsilon}_r = \begin{bmatrix} \epsilon_d & 0 & 0 \\ 0 & \epsilon_{md} & -\epsilon_{off} \\ 0 & \epsilon_{off} & \epsilon_{md} \end{bmatrix}. \quad (2.69)$$

- \mathbf{B}_y :

$$\hat{\epsilon}_r = \begin{bmatrix} \epsilon_{md} & 0 & \epsilon_{off} \\ 0 & \epsilon_d & 0 \\ -\epsilon_{off} & 0 & \epsilon_{md} \end{bmatrix}. \quad (2.70)$$

- \mathbf{B}_z :

$$\hat{\epsilon}_r = \begin{bmatrix} \epsilon_{md} & -\epsilon_{off} & 0 \\ \epsilon_{off} & \epsilon_{md} & 0 \\ 0 & 0 & \epsilon_d \end{bmatrix}. \quad (2.71)$$

For diagonal elements ε_d , magnetic diagonal elements ε_{md} and for off-diagonal elements ε_{off} we write

$$\varepsilon_d = \varepsilon_\infty - \frac{\omega_p^2}{\omega(\omega - i\gamma)} + \frac{A\omega_L^2}{\omega_L^2 - \omega^2 - i\omega\gamma_L}, \quad (2.72)$$

$$\varepsilon_{md} = \varepsilon_\infty - \frac{\omega_p^2(\omega^2 + i\gamma_D\omega)}{(\omega^2 + i\gamma_D\omega)^2 - \omega_c^2\omega^2} + \frac{A\omega_L^2}{\omega_L^2 - \omega^2 - i\omega\gamma_L}, \quad (2.73)$$

$$\varepsilon_{off} = -i \frac{\omega_p^2\omega_c\omega}{(\omega^2 + i\gamma_D\omega)^2 - \omega_c^2\omega^2}. \quad (2.74)$$

Parameters ω_p , ω , γ_D were described before; the cyclotron frequency ω_c is defined as

$$\omega_c = \frac{eB_x}{m_e}. \quad (2.75)$$

The diagonal components of the permittivity cause the plasmonic behavior, and the off-diagonal components are responsible for non-symmetrical response with the change of the orientation of the external magnetic field [29].

3 Finite Element Method in COMSOL Multiphysics

Analytical solutions tend to be restricted to regular geometries and simple boundary conditions. In more complicated physical problems the numerical simulations are practical and needed.

The description of the laws of physics for space-dependent and time-dependent problems are mostly expressed in terms of partial differential equations. Instead of analytical method, we use different types of discretizations that approximate the partial differential equations with numerical model equations, which can be solved using numerical methods [30].

The finite element method (FEM) is a technique for finding approximate solutions to boundary value problems of mathematical physics. FEM has been developed and applied extensively to problems of structural analysis and problems of other fields and subdivides a large (physical) problem into smaller simpler parts called finite elements. One of the benefits of using the FEM is that it offers great freedom in the selection of discretization in the elements that may be used to discretize space and the basis functions. The solution of the boundary value problems that arise in the mathematical modeling of physical systems, has long been a major topic in mathematical physics and the most widely used methods are the Ritz (Rayleigh-Ritz) method and the Galerkin method [31, 30].

3.1 Basic principles of FEM

The finite element method is a numerical technique designed to seek approximate solutions to problems described by a system of partial differential equations (PDEs), reducing them to a system of algebraic equations.

First, we discretize the problem in a proper number of elements and then we find solutions in specific points of those elements which are called nodes. Finally, the general solution is given by interpolating the solution on the nodes. The number of elements has to be considered accurately because more and smaller elements mean more precise model but the model needs more computation time which has to be taken into account.

By solving the differential equations in a domain of interest we can obtain the real solution of our problem only if the model is described properly. Every domain (except only a few special cases) is delimited by boundary which is described by

boundary conditions. To find real solution we have to know them because to complete description both differential equations and boundary conditions are needed.

The nature of this conditions depends on the physics of our problem. Generally, we distinguish between two basic types of conditions. The first, Dirichlet conditions, specifies the value of state variable at the boundary and only interior nodes in the problem are unknown. The second condition – Neumann condition – specifies the normal derivative of the state variable and can be implemented by adding additional equations at the boundary. Other boundary conditions can be more complicated. For example, Perfectly matched layer (PML) is a type of absorbing boundary condition for wave equations which act as a lossy material (or layer) and is used for perfect absorptions and domain isolation.

At the start, our physical problem is expressed in the strong form and then is translated in the variational form (which is also called weak form) to solve. The first step of variational methods that reduce the original problem in variational form is finding the energy functional of the problem. The finite element methods obtains the correct solution for any finite element model by minimizing an energy functional. Based on the law of conservation of energy the energy functional must equal to zero.

In general, the application of the FEM involves followings [32]:

1. Discretization or subdivision of the domain.
2. Defining the governing algebraic equations for a generic element.
3. Formulation of the system of equations (Ritz or Galerkin method), assembling of all elements in the solution region and determination of the total energy.
4. Solution of the system of equations.

The first step, which can be completely separated from the other steps and usually is considered as a preprocessing, is perhaps the most important step because the manner in which the domain is discretized will affect the accuracy of the numerical results. For one dimensional domain, the elements are often short line segments. For a two dimensional domain, the elements can be triangles or rectangles. Triangular elements fill better the surfaces of the most varied forms while rectangular ones are best suited for discretizing rectangular regions. In a three dimensional case, the domains are subdivided into triangular prisms, tetrahedra or rectangular bricks. Tetrahedra elements are the simplest and best suited for arbitrary-volume domains. If the boundary is curved, the elements represent only an approximation of the original geometry [32].

3.2 Weak formulation of a waveguide

In this section, we illustrate how to obtain the weak formulation of dielectric rectangular waveguide with sides of length x_1 and x_2 . This process corresponds to the point two in the previous page and is executed directly by the software in COMSOL Multiphysics.

As a generic element we take a cross-section Ω with specified boundary conditions. Our governing equation is the wave equation (2.15).

We start from the wave equation which is for clarity rewritten to form

$$\Delta u(x_1, x_2, t) - \frac{1}{c^2} \frac{\partial^2 u(x_1, x_2, t)}{\partial t^2} = 0 \quad (3.1)$$

in $\Omega \in \mathfrak{R}$, where Ω is the area of cross section, with the Dirichlet boundary condition $u(\mathbf{x}, t) = 0$ on $\Gamma \in \mathfrak{R}$, where Γ is the boundary of the area Ω . We need to find a solution in a form $u(\mathbf{x}, t) = \hat{u}(\mathbf{x}, t)e^{i\omega t}$, so by the introducing the relation

$$\frac{\partial^2 u}{\partial t^2} = \hat{u}(\mathbf{x}) \cdot e^{i\omega t} \omega^2 \quad (3.2)$$

to the wave equation (3.1) we get our problem in the form

$$\Delta \hat{u}(\mathbf{x}) = -\frac{\omega^2}{c^2} \hat{u}(\mathbf{x}) \quad (3.3a)$$

$$\hat{u}(\mathbf{x}) = 0 \quad (3.3b)$$

For a derivation of the weak formulation of (3.3) we use the Green's theorem

$$\int_{\Omega} \sum_i \left(\frac{\partial u}{\partial x_i} \cdot v + u \cdot \frac{\partial v}{\partial x_i} \right) dx_i = \int_{\Gamma} \sum_i u \cdot v \cdot n_i dS. \quad (3.4)$$

Left side of the equation (3.3a) we multiply by the test function $v(\mathbf{x})$, integrate over the area Ω

$$\int_{\Omega} \Delta \hat{u}(\mathbf{x}) \cdot v(\mathbf{x}) \cdot dx = \int_{\Omega} \sum_i \frac{\partial}{\partial x_i} [\nabla \hat{u}(\mathbf{x})]_i \cdot v(\mathbf{x}) dx \quad (3.5)$$

and apply Green's theorem

$$\begin{aligned} & \int_{\Omega} \sum_i \frac{\partial}{\partial x_i} [\nabla \hat{u}(\mathbf{x})]_i v(\mathbf{x}) dx = \\ & = \sum_i \left\{ \int_{\Gamma} [\nabla \hat{u}(\mathbf{x})]_i \cdot v(\mathbf{x}) \cdot n_i \cdot dS + \int_{\Omega} [-\nabla \hat{u}(\mathbf{x})]_i \cdot \frac{\partial v(\mathbf{x})}{\partial x_i} dx \right\}. \end{aligned} \quad (3.6)$$

The first term is equal to zero since the test function condition is $v(\mathbf{x}) = 0$, and for the second term, we write

$$-\int_{\Omega} \sum_i \frac{\partial \hat{u}(\mathbf{x})}{\partial x_i} \cdot \frac{\partial v(\mathbf{x})}{\partial x_i} dx = -\int_{\Omega} \nabla \hat{u}(\mathbf{x})_i \cdot \nabla v(\mathbf{x}) dx. \quad (3.7)$$

Now, for the right side of the equation (3.3a), we proceed in the same way

$$\int_{\Omega} -\left(\frac{\omega}{c}\right)^2 \cdot \hat{u}(\mathbf{x}) \cdot v(\mathbf{x}) \cdot d\mathbf{x} = -\int_{\Omega} \lambda_i \hat{u}(\mathbf{x}) \cdot v(\mathbf{x}) \cdot d\mathbf{x} \quad (3.8)$$

and compare it with the left side

$$-\int_{\Omega} \nabla \hat{u}(\mathbf{x}) \cdot \nabla v(\mathbf{x}) \cdot d\mathbf{x} = -\int_{\Omega} \lambda_i \hat{u}(\mathbf{x}) \cdot v(\mathbf{x}) \cdot d\mathbf{x}. \quad (3.9)$$

We are looking for the eigennumber $\lambda = K^2$ and the eigenvector $\hat{u} \neq 0$ of

$$V := \{v : \Omega \rightarrow \Re \mid \int_{\Omega} v^2 < \infty; \int_{\Omega} \|\nabla v\|^2 < \infty; v = 0 \text{ on } \Gamma\} \quad (3.10)$$

$$\int_{\Omega} \nabla \hat{u}(\mathbf{x}) \nabla v(\mathbf{x}) dx = K^2 \int_{\Omega} \hat{u}(\mathbf{x}) \cdot v(\mathbf{x}) dx \quad \forall v \in V := H_0^1(\Omega),$$

which is the weak formulation of the rectangular waveguide. In the next steps the weak formulation is transferred to the matrix form to obtain local matrices. All these steps are done by software in COMSOL Multiphysics.

3.3 Modeling in COMSOL Multiphysics

COMSOL Multiphysics software is a powerful finite element and partial differential equation solution engine with integrated modeling environment which provides multi-physics modeling. Generally, there are five stages in setting up a model in COMSOL Multiphysics [33]:

- **Geometry modeling:** Geometry operations are organized in a parametric sequence of operations in the Model Tree. COMSOL Multiphysics enables 1D, 2D and 3D geometry modeling with native geometry kernel. For more complicated models boolean operations can be used such as union, difference and intersection. All models can be created in external CAD systems and imported.

Although COMSOL Multiphysics fully supports 3D geometries the simplifica-

tion to 2D geometry with use of symmetries is desirable if is possible. This is because 3D models require more computer memory and time to solve. Moreover, the solutions in 2D are often more accurate because much denser mesh can be used. But not every model can be expressed as a two dimensional. The need of modeling of some structures in 3D was shown by doc. Richter in his work dealing with advanced subwavelength photonic and plasmonic waveguide nanostructures [34].

- **Mathematical equations and properties definition:** Specifying the equations satisfied internally within the geometries (subdomain physics) and those on the boundaries or vertices (boundary and point physics). For defining materials and properties the library of predefined materials and chemical elements is available. COMSOL Multiphysics provides several physical modules with dedicated physics interfaces and tools for electrical, mechanical, chemical, fluid flow, and more applications.
- **Meshing:** COMSOL Multiphysics has powerful default automatic and semi-automatic mesh generator tools built-in. The default algorithm is automatic tetrahedral meshing for physics defined in solids and a combination of tetrahedral and boundary layer meshing for fluids. One model can contain many types of mesh, COMSOL Multiphysics permits considerable user control over customization.

Physics-controlled mesh is set as a default and is adapted to the current physics settings in the model. The mesh generator automatically generates a finer mesh where there are more geometrical details.

In various physical models, there are some problem-dependent factors that determine the required mesh resolution. In modeling of the electromagnetic wave, it is a wavelength. To proper resolution, it is necessary to use more than 10 linear elements per wavelength. In our models, we use more than 30 elements per wavelength due to the strong damping in the metal domains. The propagation length is discussed in Chapter 2.3. and is given by Equation (2.48). The detail of the mesh around the interface between metal domain and dielectric domain is shown in Figure 5.4.

- **Solving:** The physics software runs the analysis together with adaptive meshing and error control using a variety of numerical solvers. One study can hold a sequence of solvers, such as for stationary, eigenfrequency, frequency-domain and time-domain analysis.
- **Post-processing:** COMSOL Multiphysics enables to visualize almost any quantity of interest related to the simulation results. Built-in visualization tools include surface, slice, isosurface, cut plane, arrow and streamline plots, as well as graphs. Post-processing tools allow computing the maximum, minimum, average, etc. COMSOL Multiphysics provides a method of automatically creating MATLAB m-file source code. Exporting solutions to MATLAB also makes post solution analysis more flexible.

This software offers several modules (AD/DC Module, Structural Mechanics Module, Heat Transfer Module...). For simulations, we use the Radio frequency (RF) module which is optimized for the analysis of electromagnetic waves and is very useful for design antennas, waveguides, optical fibers, photonic crystals and so on. RF module offers set of boundary conditions specified for electromagnetic waves. Their use and characteristics will be discussed with the studied models.

4 Surface Plasmon Resonance

The most common approach to the excitation of the surface plasmon polaritons uses a prism coupler and the attenuated total reflection method (ATR). There are two configurations of the ATR method, Kretschmann-Raether configuration and Otto configuration, that are shown in Figure 4.1.

Among the other methods belongs e.g. electron beam excitation or grating coupling [9].

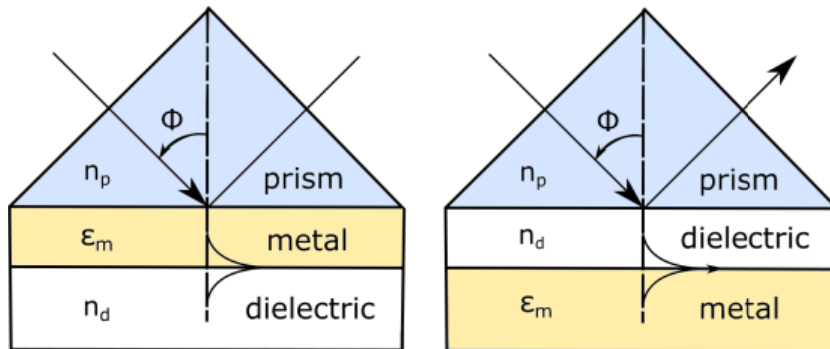


Figure 4.1: Kretschmann-Raether (a) and Otto (b) configuration.

4.1 Kretschmann-Raether configuration

In the Kretschmann-Raether configuration, the metal film is deposited directly on the prism crystal. The wave of incident infra-red light passes through a high refractive index prism (n_p) and is totally reflected at the base of the prism. A part of the light is reflected back and a part propagates in the metal film in the form of the evanescent wave.

The penetration depth of the evanescent wave is typically tens of nanometers so if the film is sufficiently thin, the wave penetrates it and couples with a surface plasmon at the outer side of the film.

The surface plasmon propagates along film with the propagation constant β that is influenced by the presence of the dielectric on the outer side of the film [35]. So that the coupling between the evanescent wave and the surface plasmon can exist, the propagation constant of the wave β_{EW} and of the surface plasmon β have to be equal [35]. For each wavelength, the matching condition is satisfied for a single angle of incidence ϕ which increases with decreasing wavelength

$$\frac{2\pi}{\lambda} n_p \sin\phi = \Re\epsilon(\beta) = \beta_{EW}, \quad (4.1)$$

where λ is the wavelength of the incident electromagnetic wave [36]. In the process of optical excitation of surface plasmon polariton, a portion of the energy of the electromagnetic wave is transferred into the energy of a surface plasmon and dissipated in the metal film which results in a drop of intensity of the light wave as we can see in the Figure 4.4.

Our model consists of three layers - air, gold (thickness 50 nm) and silica (SiO₂) layer. We use the permittivity of gold obtained from *Johnson and Christy* $\epsilon_{Au} = -11.74 - 1.2611i$ [28] and the refractive index of silica $n_s = 1.5426$ obtained from *Ghosh* [37]. The wavelength of Helium-Neon laser ($\lambda = 632.8 \text{ nm}$) has been considered. The wave vector \mathbf{k}_1 and \mathbf{k}_3 with x - and y - components has to be defined as shown in the Table 4.1.

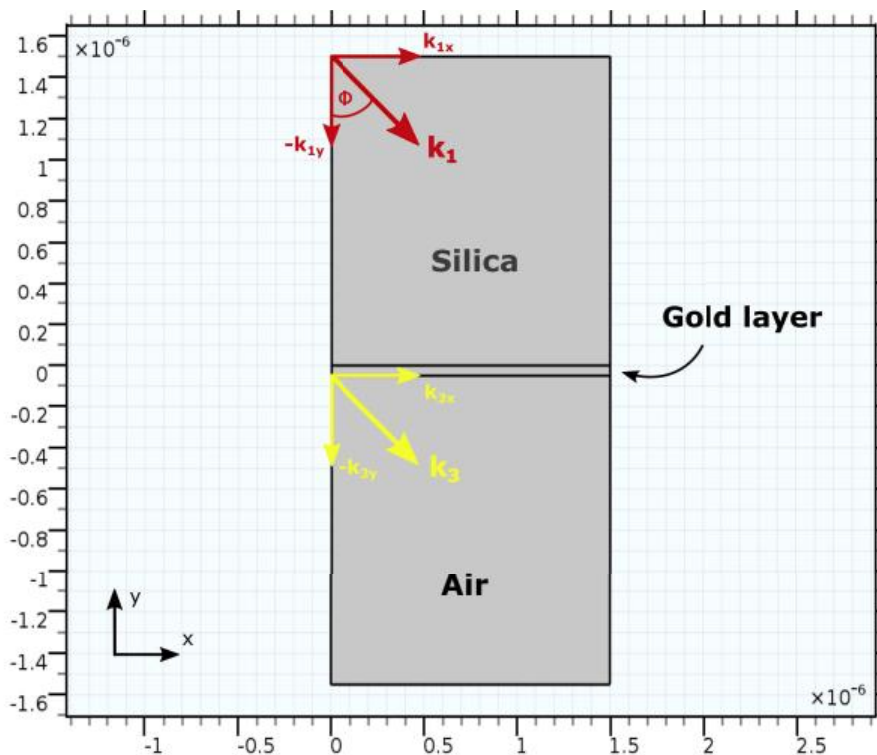


Figure 4.2: Geometry of the Kretschmann-Raether configuration

Electromagnetic Waves, Frequency Domain physics is used to solve governing Maxwell's equation in frequency domain

$$\nabla \times \frac{1}{\mu_r} (\nabla \times \mathbf{E}) - k_0^2 (\epsilon_r - \frac{j\sigma}{\omega\epsilon_0}) \mathbf{E} = 0. \quad (4.2)$$

Electric field components are solved for *In-Plane* as the electric field components are in the modeling plane and there is no electric field perpendicular to the plane. *User*

defined *Port* boundary conditions are applied on the upper and the lower boundary. Wave excitation is "On" on the upper boundary to launch the guided wave, and "Off" at the lower boundary to avoid back-reflection and to absorb perfectly all electromagnetic waves. There is no reflection directly on any port. The waves on the *Port 1* and *Port 2* are defined by *Magnetic mode field* $H_0 = e^{-i \cdot k_{1x} \cdot x}$ with the propagation constant $\beta = |k_{1y}|$ ($H_0 = e^{-i \cdot k_{3x} \cdot x}$ with the propagation constant $\beta = |k_{3y}|$, respectively). The use of *Ports* on the upper and lower boundary is necessary to obtain scattering parameters (S-parameters) which are complex-valued, frequency dependent matrices describing the reflection (and transmission) of electromagnetic waves at different ports of devices. For our problem with two ports, the S-parameters are

$$S = \begin{bmatrix} S_{11} & S_{12} \\ S_{21} & S_{22} \end{bmatrix}, \quad (4.3)$$

where S_{11} is the input port voltage reflection coefficient, S_{21} is the reverse voltage gain (the voltage transmission coefficient from Port 1 to Port 2), S_{12} is the forward voltage gain and S_{22} is the output port voltage reflection coefficient. By $|S_{ij}|^2$ the time average power reflection (or transmission) coefficients can be obtained [38]. The reflectance computed with the use of S-parameters is shown in Figure 4.4.

On the left and right boundaries are applied *Periodic Condition* with *Floquet periodicity* which is typically used for models involving plane waves interacting with periodic structures [38].

Table 4.1: List of variables for Kretschmann-Raether and Otto configuration

Name	Expression	Unit
k_1	$n_p k_0$	rad/m
k_{1x}	$k_1 \sin \phi$	rad/m
k_{1y}	$-k_1 \cos \phi$	rad/m
k_3	$(n_d k_0)^2 - k_{3x}^2$	1/m ²
k_{3x}	k_{1x}	rad/m
k_{3y}	$\Re(k_3) < 0, \Im(k_3) = 0 : -i\sqrt{k_3}$ else : $\sqrt{k_3}$	1/m

For computing the reflectance, we use the mesh which is depicted in Figure 4.3. Several meshes are needed. *Edge* mesh, *Copy edge* mesh which makes possible to copy the mesh from already meshed entity to an unmeshed entity and *Free Triangular* mesh. For computing the field profiles near the interface between the metal and

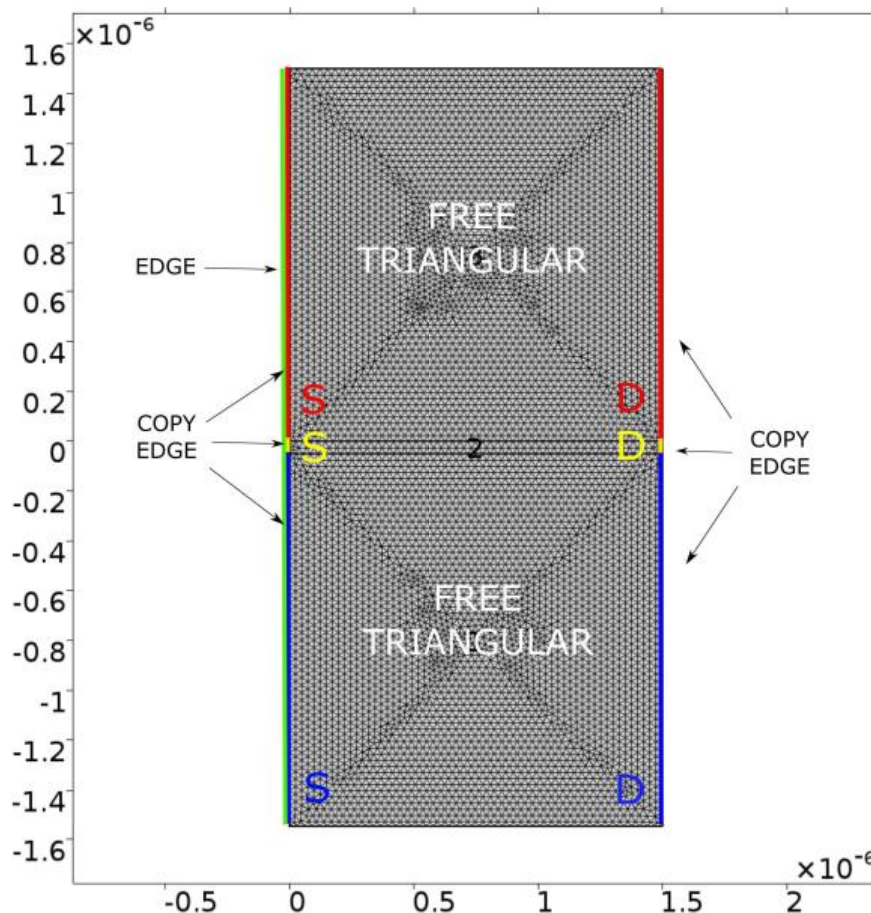


Figure 4.3: Meshing of Kretschmann-Raether configuration for computing the reflectance. Several types of mesh were used: Edge mesh, Copy edge mesh, and Free Triangular mesh. Letters S and D indicate the source and the destination boundary for Copy Edge meshes.

the dielectric we add the *Boundary Layers* mesh and another *Free triangular* mesh to the metal domain with high resolution of approximately 50 nodes per wavelength.

Study set up consists of *Parametric Sweep* over the angle of incidence and *Frequency Domain* study. The range of angle values starts at 35 degrees and with a step 0.02 degree and ends at 50 degrees.

Figure 4.4 shows the reflectance as a function of the angle of incidence. We can see that the curve has the minimum just under 44 degrees, specifically at 43.73 degrees, which indicates the existence of the plasmon. The result from COMSOL Multiphysics is at good agreement with the analytical results from MATLAB where the equations (2.25b), (2.27) and (2.30) were used. Figures 4.5 and 4.6 shows the dependence of the x component of the electric field and z component of the magnetic field on the angle of incidence, respectively. In Figures 4.5(a) and 4.6(a) we can see

that the incident electromagnetic wave is reflected, there are no plasma resonances and the energy is concentrated in the prism. With increasing angle of incidence, more energy is concentrated in the dielectric. When the angle reaches the $\lambda = 43.73$ degrees, the coupling is the strongest and we can observe surface plasmon resonance. The minimum amount of the energy is concentrated in the prism as is depicted in Figures 4.5(e) and 4.6(c). These figures corresponds with the minimum of the reflectance in the Figure 4.4. Another increasing of the angle of incident causes that the plasmon ceases to exist and the wave is reflected again as is illustrated in Figures 4.5(i) and 4.6(f).

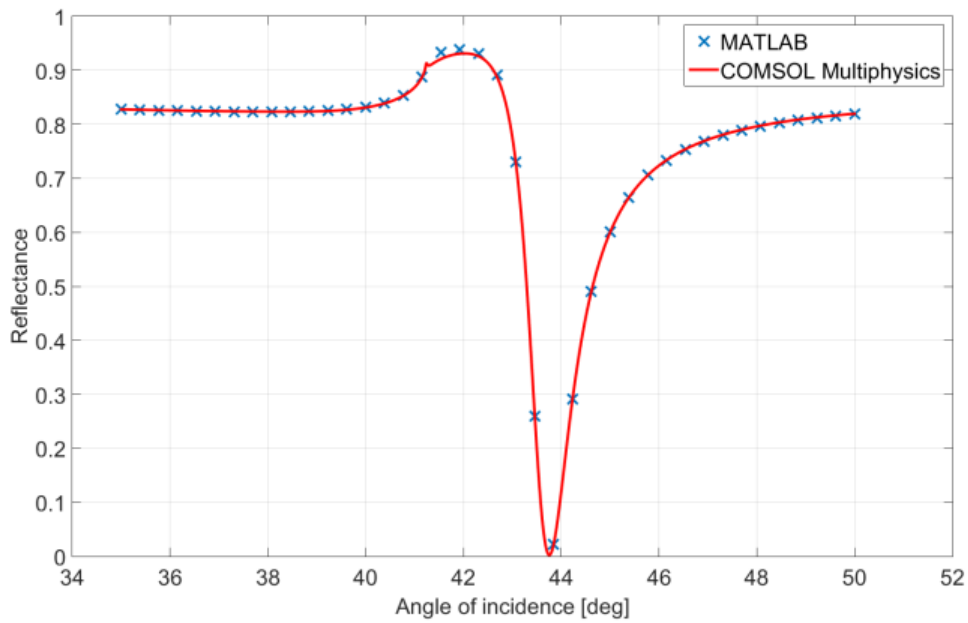


Figure 4.4: Reflectance as a function of the angle of incidence in Kretschmann-Raether configuration. The drop of the intensity of the reflected wave is caused by excitation of surface plasmon polariton. Data computed by COMSOL Multiphysics are compared against the analytical results obtained from MATLAB.

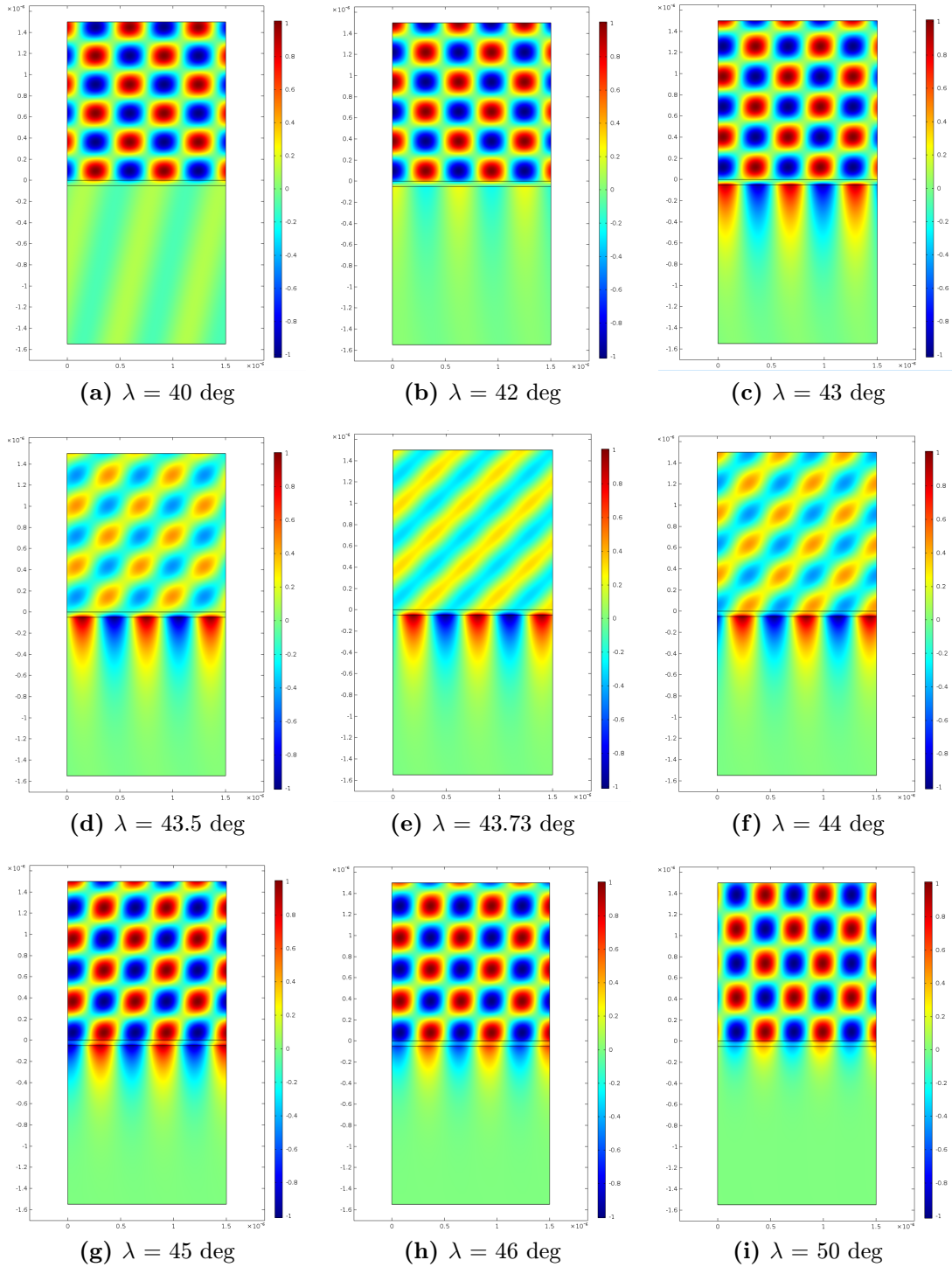


Figure 4.5: Dependence of the electric field (x component) on the angle of incidence. Figure (e) agrees with the minimum of the reflectance (depicted in Figure 4.4) where the plasmon exists.

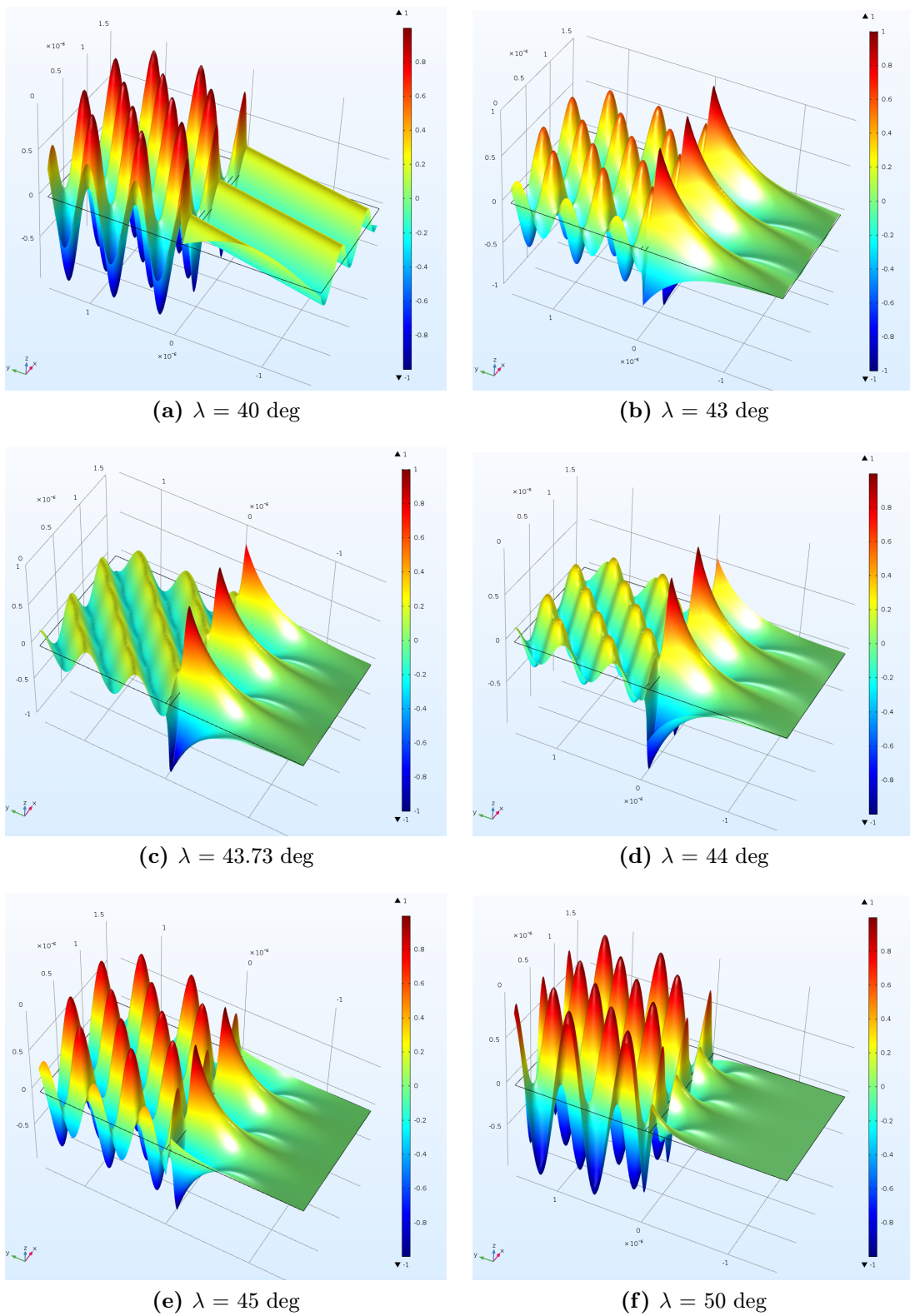


Figure 4.6: Dependence of the magnetic field (z component) on the angle of incidence. Figure (c) agrees with the minimum of the reflectance (depicted in Figure 4.4) where the plasmon exists.

4.2 Otto configuration

In contrast with the Kretschmann-Raether configuration, in the Otto configuration there is a distance between the metal and the prism. This space is filled with a lower refractive index medium, so we can say that the prism is interfaced with a dielectric-metal waveguide which consists of a thin dielectric film and a semi-infinite metal.

The electromagnetic wave incidents on the prism-dielectric film interface with the angle that is larger than the critical angle for these two materials. The produced evanescent wave propagates along the interface between the prism and the film. The wave and surface plasmon at the dielectric-metal interface can couple if the thickness of the film is chosen properly. Likewise the Kretschmann-Raether configuration, the coupling can occur if the propagation constants of the evanescent wave and of the surface plasmon are equal [35].

The set up in COMSOL Multiphysics for Otto configuration is very similar to the set up of Kretschmann-Raether configuration (same physics and meshing, analogous geometry). In this section, we study the behavior of Otto configuration for different gap width.

Our model geometry consists of three layers as before, but the material of the middle layer is air which is surrounded by the glass and the gold. We use the frequency of He-Ne laser, and for comparison with the previous model we set the angle of incidence to the 43.73 degrees.

With respect to the architecture of the Otto configuration, we set *Parametric Sweep* over the thickness of the air layer from 450 *nm* to 650 *nm*. The dependence of the reflectance to the thickness of this layer is depicted in Figure 4.7. As shown, the minimum of the reflectance is for the thickness 542 *nm*. In Figures 4.8 and 4.9 we can observe the penetration of the magnetic field to the gold region which is less than 100 *nm*.

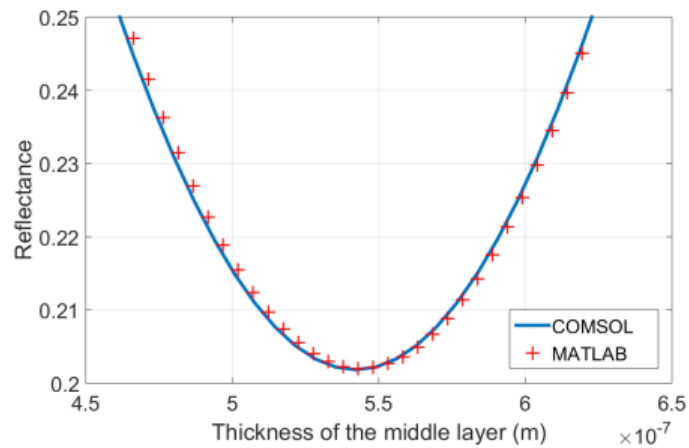


Figure 4.7: Dependence of the reflectance to the thickness of the middle layer for the angle of incidence of 43.73 degrees. Result obtained by Comsol (blue line) is compared with an analytic result (red crosses).

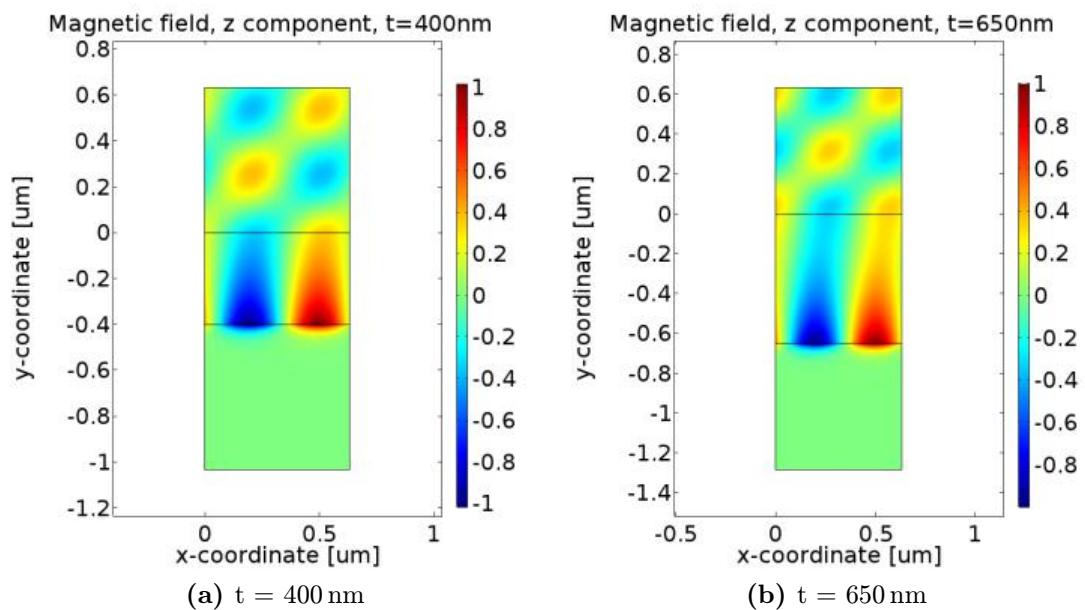


Figure 4.8: Dependence of the magnetic field (z component) on the thickness of the air layer for Otto configuration. The upper layer is the silica layer, the middle is the air layer, and the lowest is the gold layer. The penetration of the magnetic field to the metal layer is explicit.

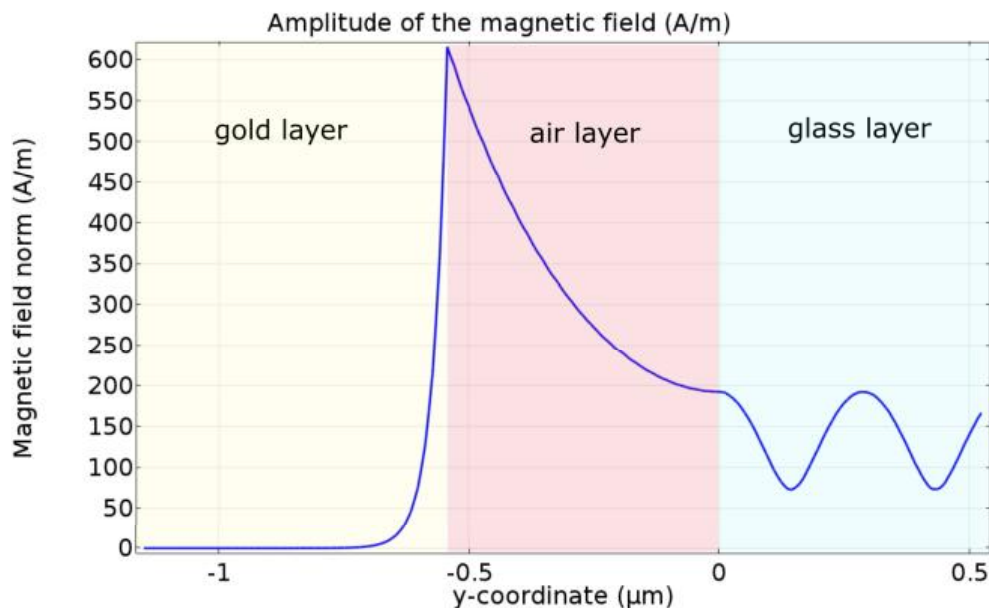


Figure 4.9: Amplitude of the magnetic field calculated on the cross-section of the Otto configuration for the thickness of the air layer $t = 542 \text{ nm}$ where the minimum of reflectance occurs. We can observe the penetration of the magnetic field to the gold layer.

Otto configuration with external magnetic field

According to experiment by *Chochol et al.* [29] we apply external magnetic field to shift the frequency position of the plasmonic resonance. In this configuration we use the same architecture as in the experiment. As a conductor we use InSb with parameters given in Table 4.2, the angle of incidence is $\alpha = 35$ degrees and the wavelength of the electromagnetic wave is $\lambda = 650 \text{ nm}$. The thickness of the middle layer is 23.4 nm . The refractive index of the first dielectric layer (silicon prism) is $n_1 = 3.4164$ and of the second dielectric layer is $n_2 = 1.625$.

Table 4.2: List of material parameters for InSb [29]

ω_p rad/s	γ_L s^{-1}	γ_D s^{-1}	ω_L rad/s	A_L -	ϵ_∞ -	m_e kg
$5.58 \cdot 10^{13}$	$5.3 \cdot 10^{11}$	$1.938 \cdot 10^{12}$	$3.37 \cdot 10^{13}$	1.9484	15.386	$1.5395 \cdot 10^{-32}$

The InSb material is loaded to the COMSOL Multiphysics with the use of *Analytic Functions*. We define the Drude-Lorentz model (see Equation 2.72) as a function which depends on the frequency and, in the next step in defining the physics,

we put this function to *Wave equation* for description of the permittivity of the InSb domain.

External magnetic field can be added to the model through the equations discussed at the end of Chapter 2.4. We define new function for each of all five components of the relative permittivity tensor $\hat{\varepsilon}_r$ given by Equation (2.71). In the *Wave equation* we choose *User defined Anisotropic* relative permittivity where we set the proper form of the tensor $\hat{\varepsilon}_r$. The magnetic flux density B_z was added as a new parameter that is a part of the cyclotron frequency ω_c (see Equation (2.75)). We observe the changes in the surface plasmon resonance for the external magnetic field $B_z = \pm 0.25 T$ in the transversal configuration.

In Figure 4.10 are illustrated the results computed by COMSOL Multiphysics which are in good agreement with the experimental data (cross lines) obtained by *Chochol et al.* [29]. As it shown, the external magnetic field has strong effect to the InSb. The positive value of the magnetic flux density causes the strong shift to the lower values of wavenumber (about 5 cm^{-1}) and vice versa. The corresponding value of shift in the frequency range is more than 100 GHz . The application of the magnetic field can be used in the semiconductor based SPR THz sensors for tuning the surface plasmon resonance, so we are able e.g. to find stronger coupling of SPR for selected thickness and refractive index of the dielectric [29].

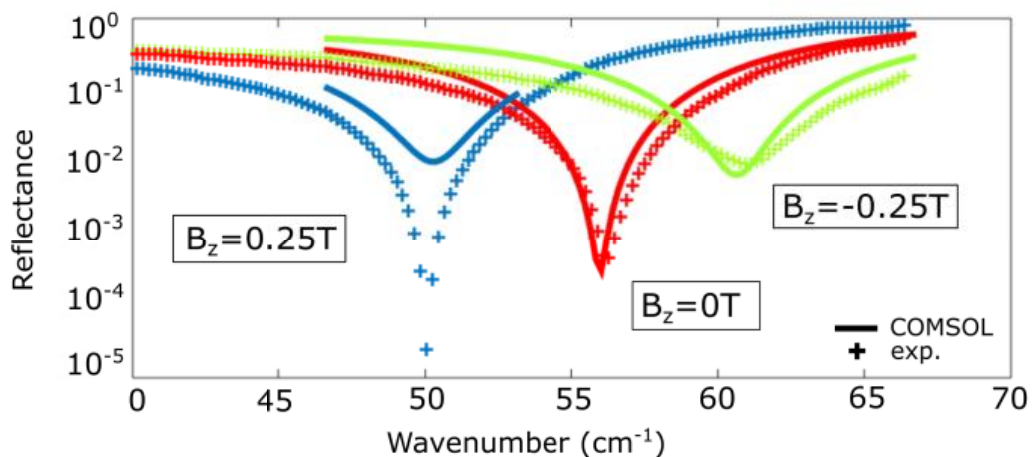


Figure 4.10: The effect of the magnetic flux density B_z to the surface plasmon resonance in the Otto configuration for InSb. Experimental data are obtained by permission from *Chochol et al.* [29].

5 Plasmonic Waveguides

In this chapter, basic plasmonic waveguides will be investigated. Development of metal waveguides is one of the straightforward applications of surface plasmons. These waveguides have a great potential e.g. for telecommunications as a circuit interconnections or for subwavelength circuitry as key elements [39].

There are numerous waveguide architectures, such as layered structures, metallic nanowires, metallic nanoparticle arrays, hybrid wedge plasmonic waveguides, available in the literature [40, 41] which utilizes the concept of surface plasmon polaritons by storing part of light's energy as electron plasma oscillation at the interface between metal and dielectric.

Plasmonic waveguides with ability to confine light at sub-wavelength scale have a large number of applications in the field of nanophotonic devices [42], biological and chemical sensors [35], holography [43] and other that we mentioned in Chapter 1.

5.1 Planar waveguides

There are two types of basic planar plasmonic waveguides that will be discussed in this section. The structure consists of a thin metal film sandwiched between two dielectric media is called dielectric–metal–dielectric (DMD) or insulator–metal–insulator (IMI) waveguide. This waveguide can support two TM modes in case that the metal film is much thicker than the penetration depth of a surface plasmon at each metal/dielectric interface which corresponds to two surface plasmons at the opposite boundaries of the metal film.

Coupling between two surface plasmons occurs with a decrease of the thickness. For any thickness of the metal film there are two coupled surface plasmons which are referred as to symmetric and antisymmetric surface plasmons based on the symmetry of the magnetic field distribution. The symmetric mode exhibits a lower attenuation than antisymmetric and as referred is to a long-range surface plasmon, while the antisymmetric mode is referred to a short-range plasmon. At certain metal film thickness we can observe the mode cut-off when the symmetric mode ceases to exist as a guided mode [35].

Metal–dielectric–metal (MDM) structure (or metal–insulator–metal MIM) is complementary to the structure described above. Since the field is bounded by metal layers and absolute values of the real parts of the permittivity of the metal are quite large, the penetration of the field into the metal layer is small [40].

These types of waveguides were investigated many times as well as possibilities of modeling them with the use of numeric methods. Very good and precise analysis a of MIM and IMI waveguides in COMSOL Multiphysics and comparisons with the analytical solutions was presented by *Yushanov et al.* in COMSOL conference in Boston in 2015 [44]. Further, *Y. Chowdhury* presented a comprehensive study of plasmonic waveguides and their design in COMSOL Multiphysics [45]. We have selected MIM structure as an example of the surface plasmon planar waveguide.

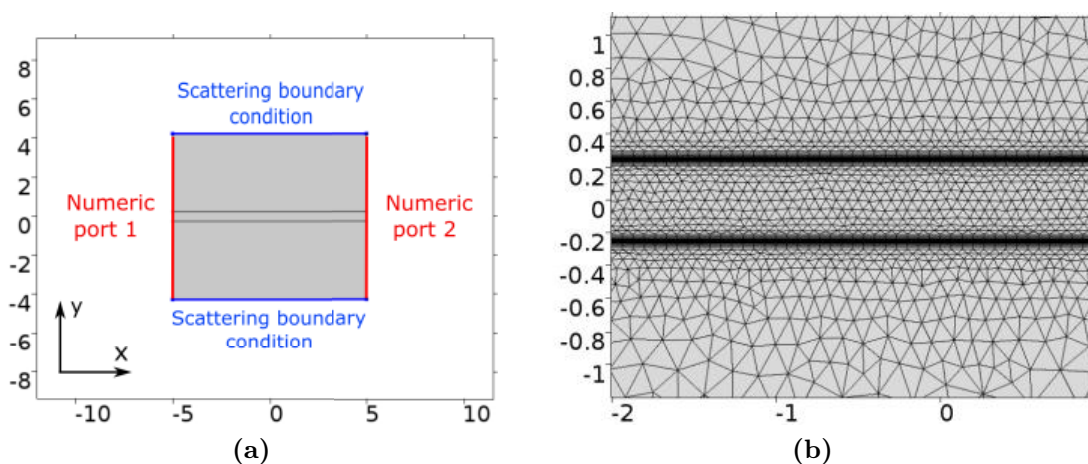


Figure 5.1: (a) Structure of the MIM and IMI planar waveguides with used boundary conditions. (b) Detail of the mesh. *Boundary Layers* and two *Free Triangular* meshes were applied. Axis represent the width and length in μm .

The architecture of the MIM waveguide consists of two metal layers and one dielectric layer which is sandwiched between them. The model is studied in the longitudinal cross section and is infinite in the z - direction. As materials we use the silica obtained from *Ghosh* [37] and the gold obtained from *Johnson and Christy* [28]. These materials were input to the model through the *Interpolation functions*.

The *Electromagnetic Waves* and *Frequency Domain* is used as in the previous models. On the left boundary we apply the *Numeric Port* with the wave excitation "On" because the wave is launched here. On the opposite side we apply the same *Numeric Port* but we set the wave excitation to "Off". On the upper and lower boundary we apply *Scattering Boundary condition* and set *No incident field*. The application of *Numeric Ports* requires *Boundary Mode Analysis* for each of them. This type of study determines the electric field on the port boundary and finds waves that propagate in a direction normal to the port. *Boundary Mode Analysis* steps are followed by *Frequency Domain* which is the final step. The distribution of the

electric and the magnetic field is illustrated in Figure 5.2. All three figures show the attenuation of the guided mode. The mode penetrates to the metal domain but decays exponentially.

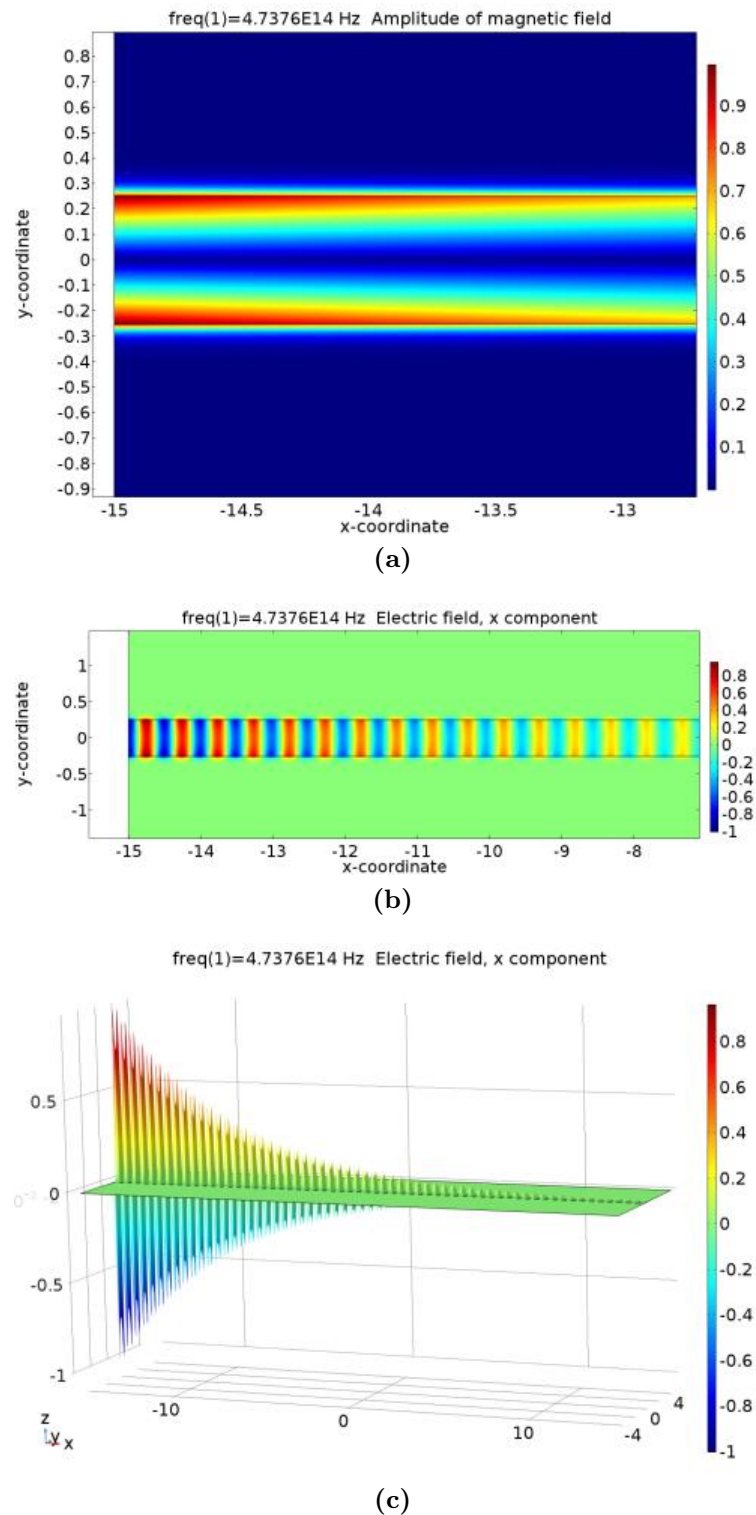


Figure 5.2: Fields distribution for the wavelength of the He-Ne laser $\lambda = 628 \text{ nm}$ for MIM structure. Figure (a) shows amplitude of the magnetic field, Figure (b) and (c) represents the electric field (x -component) distribution. The attenuation of the electromagnetic wave is noticeable as well as its penetration to the metal region.

5.2 Metal cylinder waveguides

The structure of metal cylinder waveguide is composed of a gold [28] [46] (ϵ_m) cylinder with radius r_g embedded in silica glass [37] (ϵ_d) with radius r_d and is very similar to the single dielectric-metal interface with cylindrical or curved surface. Illustration of waveguide geometry is shown in Figure 5.3, in fact, the outer radius r_d is far greater than inner radius r_g . The dimension of the waveguide in z - direction, where wave is guided, is extended to infinite.

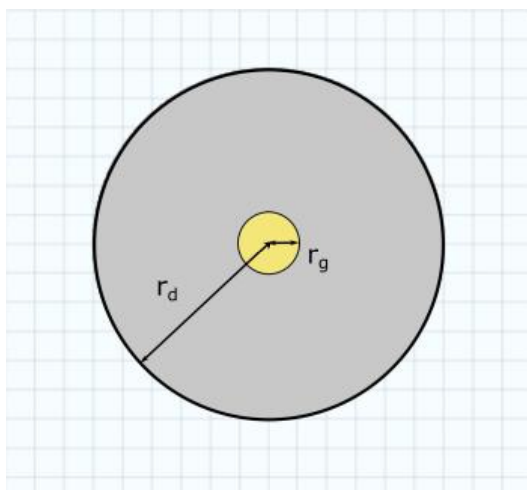


Figure 5.3: Illustration of the geometry of metal cylinder waveguide which is composed of a gold cylinder embedded in silica glass. In practice, the outer radius r_d is far greater than radius r_g .

Electromagnetic Waves, Frequency Domain physics is used. Electric field components are solved for *Three-component vector*. Electric and magnetic field of the waveguide drops off exponentially in x - and y - direction, so the fields can be assumed to be zero at some distance away from the core. At outer side of the cladding we applied *Scattering boundary condition* with no incident field. We used two *Free Triangular* meshes with different size of elements for the core and remaining domain and *Boundary Layers* mesh with respect to the frequency of the electromagnetic wave (more than 30 nodes per wavelength). Study set-up consists of only one *Mode Analysis* step. In this study COMSOL Multiphysics solves propagation constant of waveguide

$$\mathbf{E}(\mathbf{r}, t) = \Re \left\{ \mathbf{E}(\mathbf{r}) e^{j\omega t - j\beta z} \right\}, \quad (5.1)$$

where β is the propagation constant. It should be noted that in comparison with classical waveguides (e.g. photonic crystals, all-dielectric coupled silicon waveguides) they have limited propagation length (range of few μm) because of intrinsic losses

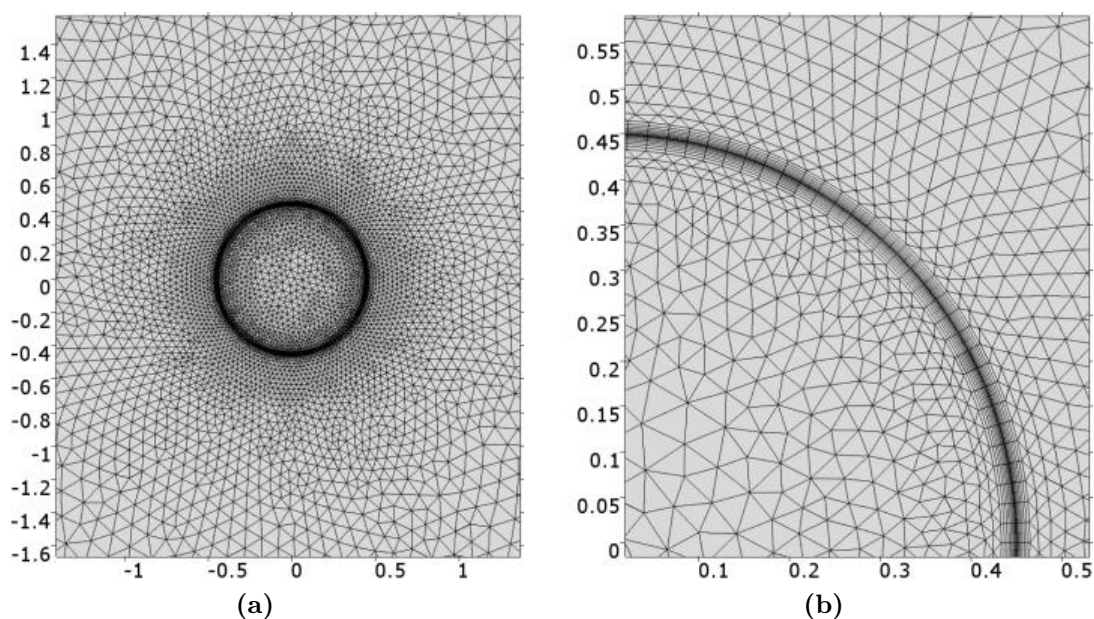


Figure 5.4: Mesh of the circular waveguide consisted of two *Free Triangular* meshes and *Boundary layers* mesh. The layers are well visible in Figure (b).

imposed by the use of metals. Operating free-space wavelength was the wavelength of He-Ne laser $\lambda_0 = 0.628\mu m$.

For the investigation of the dependence of the propagation constant β to the radius of the waveguide core r_g , we set *Parametric Sweep* from 5 nm to 350 nm. The outer radius changes proportionally. In Figure 5.5 we can see that after the radius reaches the critical value about 33 nm the propagation constant quickly begins to decrease and approaches the value of the plasmon on the planar interface. When the radius is smaller than the critical value, the symmetric mode disappears which is shown in Figure 5.7.

In Figure 5.8 the distribution of electric and magnetic field of the fundamental mode for different radii is illustrated. The fields extend into the dielectric but also to the gold core and are confined to distances that are less than free-space wavelength. With increasing radius r_g the extension to the metal region descend but the power is still confined to the circumference of the cylinder which is consistent with the graph in Figure 5.5.

For computing the dependence of the propagation constant to the wavelength of incident electromagnetic wave, we use the same geometry and same materials as in previous case. In the *Study* we set *Parametric Sweep* over the wavelength from

650 nm to 10 μm . The dispersion characteristic of the circular waveguide is shown in Figure 5.6. We can see that the fundamental mode is guided for a broad range of wavelengths but for the high wavelengths (low frequencies) is very weakly guided.

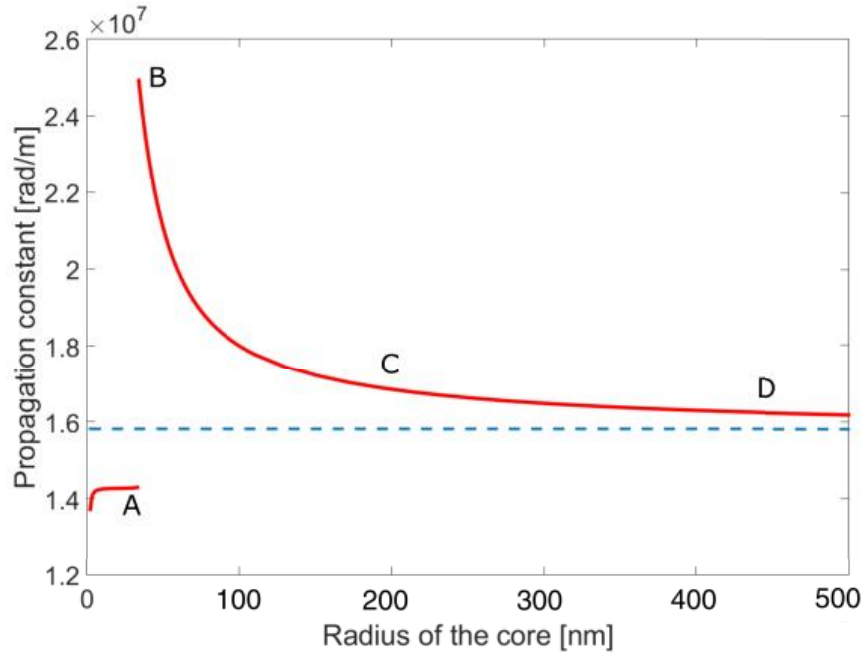


Figure 5.5: Dependence of the propagation constant β to the radius of the waveguide core. The dashed blue line represents the value of the propagation constant for the plasmon at planar interface. Profiles of electric and magnetic field in points A, B, C and D are shown in Figures 5.7 and 5.8.

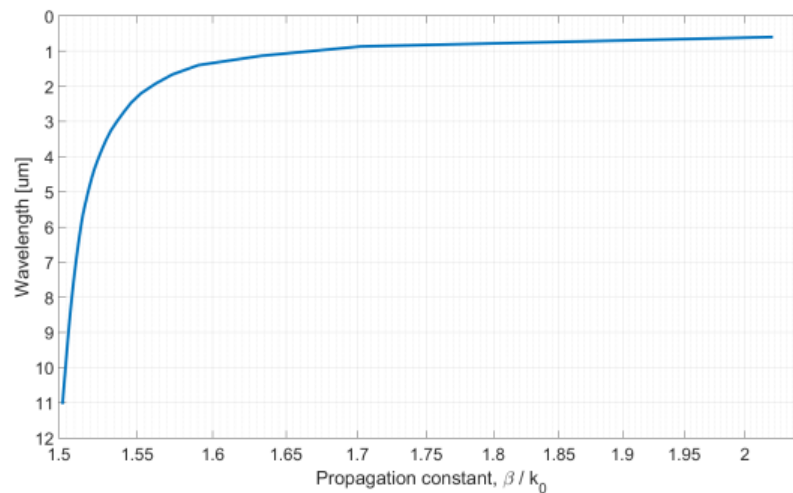


Figure 5.6: The dispersion curve for the circular waveguide. The propagation constant is decreasing function of the wavelength.

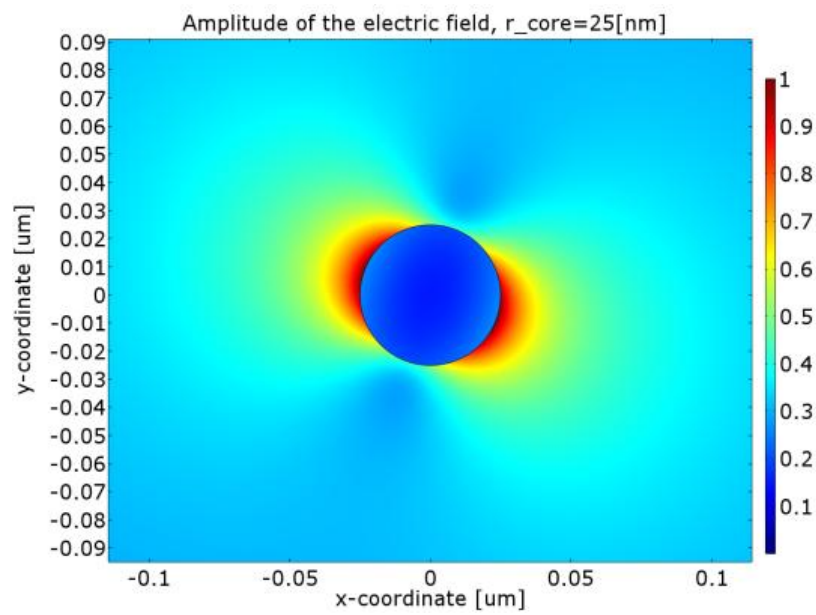


Figure 5.7: Distribution of the electric field in the waveguide for the radius of the gold core $r_g = 25 \text{ nm}$ illustrates that the symmetric mode does not exist in such small radius. The radius corresponds to the point A in Figure 5.5.

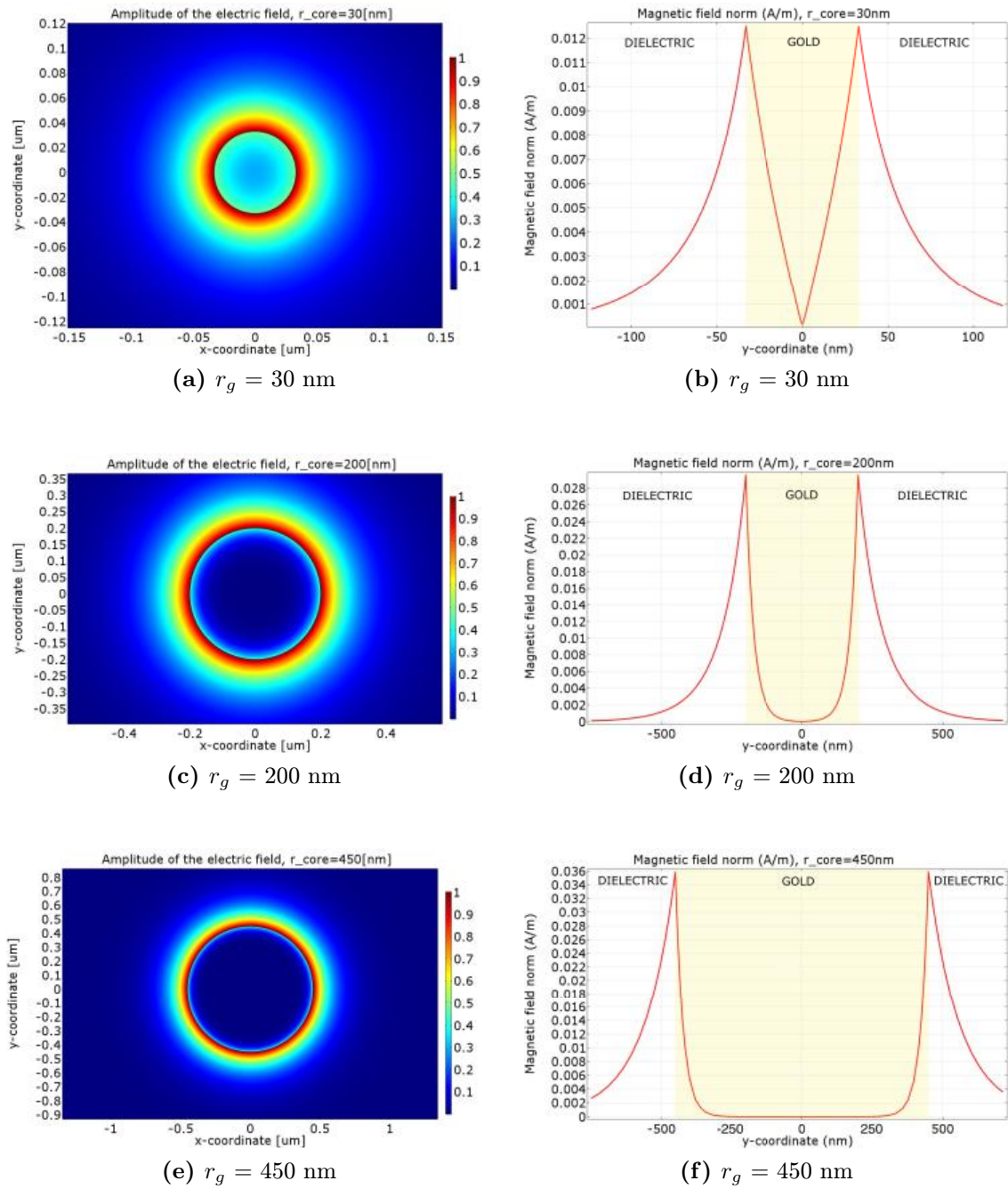


Figure 5.8: Distribution of the electric and magnetic field in the waveguide for different radius of the waveguide core. In Figures (a) and (b) we can see that the electromagnetic wave extends into the whole metal core. With the increasing radius, less wave propagates into the gold. Graphs (a) and (b) corresponds to the point B in Figure 5.5, graphs (c) and (d) to the point C and graphs (e) and (f) to the point D in the same figure.

Metal cylinder waveguide with external magnetic field

As in Chapter 4.2, we apply the external magnetic field to the metal cylinder waveguide. In this set-up we use InSb as a material of the waveguide core. The core has a radius $r_{core} = 40 \text{ nm}$, and the frequency near the minimum of the reflectance curve in Figure 4.10 that is $f = 1.6491 \cdot 10^{12} \text{ Hz}$ and that corresponds to the $k_0 = 50 \text{ cm}^{-1}$, where k_0 is the wavenumber. We apply magnetic flux density $B = 0.5 \text{ T}$ to the x direction and to the z direction as illustrated in Figure 5.9(a). External magnetic field causes the anisotropy in the InSb which is described by the relative permittivity tensor $\hat{\epsilon}_r$ given by Equation (2.71) that has been already discussed in Chapter 2.3.

Table 5.1: List of propagation constants

	$B = 0 \text{ T}$	$B_x = 0.5 \text{ T}$	$B_z = 0.5 \text{ T}$
β	$1.7238 + 0.12063i$	$1.6127 + 0.12649i$	$1.7279 + 0.12885i$

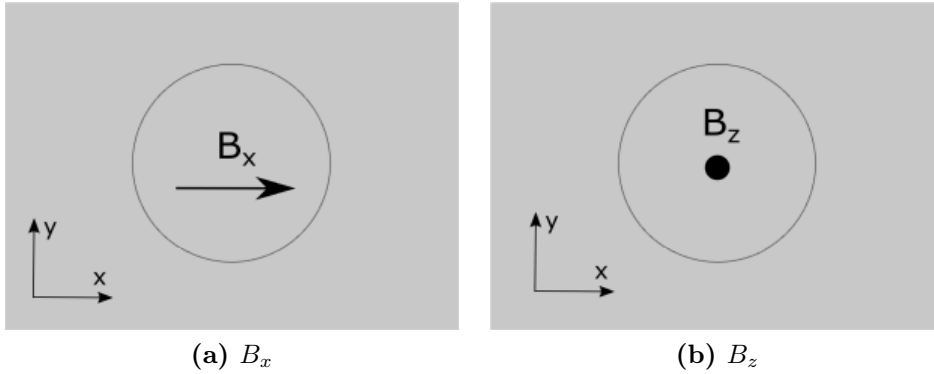


Figure 5.9: Direction of the external magnetic field.

By applying the magnetic flux density B_x to the transversal direction (Figure 5.9(a) and 5.10) we can change the propagation constant of the waveguide without greater changes in the absorption (Table 5.1) and, in addition, we can influence the distribution of the electromagnetic field in the waveguide (Figure 5.11(b)) based on the orientation of external magnetic field.

In contrast, as Figure 5.11(c) illustrates, when we apply the magnetic flux density B_z to the longitudinal direction (Figure 5.9(b)), there are no noticeable changes in the distribution of the electric field in the waveguide. Only small change in propagation constant occurs (see Table 5.1).

As we seen in Chapter 4.2 in the Otto configuration in the external magnetic field, the largest modulation of the surface plasmon properties is when the magnetic

field is in the transversal direction (perpendicular to the propagation of the surface plasmon). In the circular waveguide this would mean the magnetic field is along the circumference.

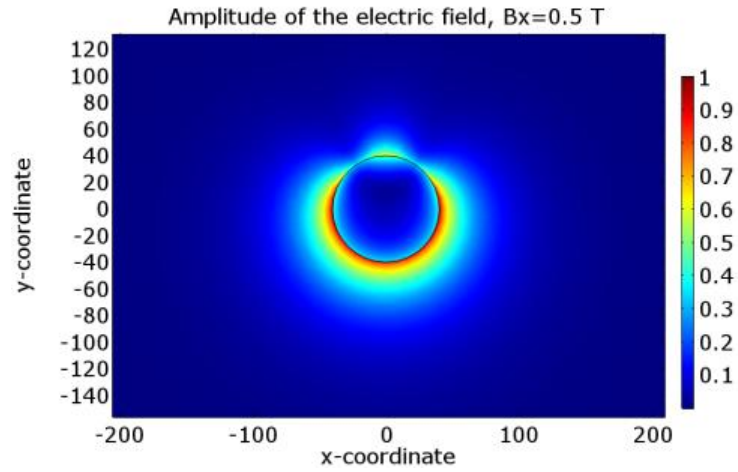


Figure 5.10: The effect of the magnetic flux density on the distribution of the electric field in the metal cylinder waveguide.

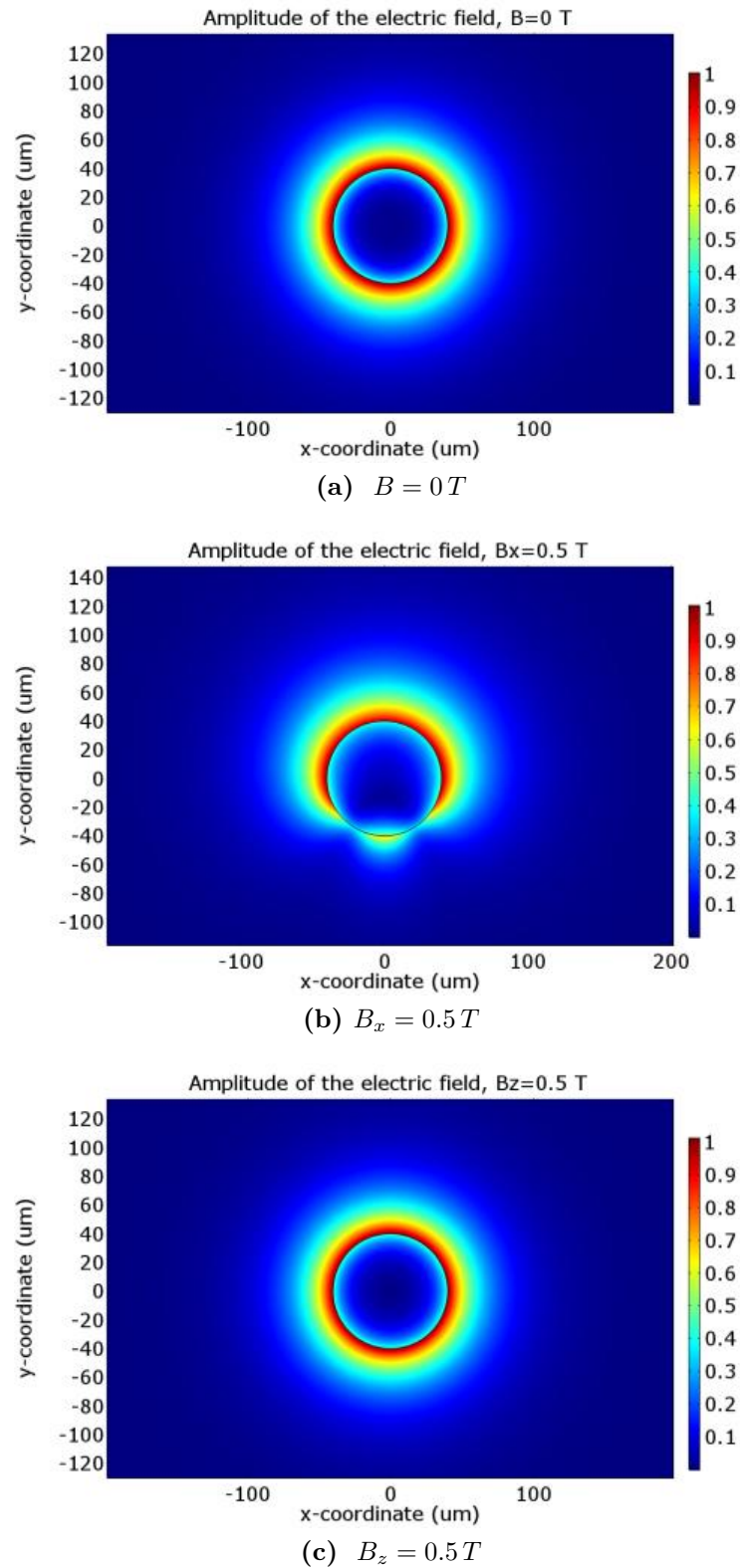


Figure 5.11: The effect of the magnetic flux density on the distribution of the electric field in the metal cylinder waveguide. The external magnetic field is in opposite direction than in Figure 5.11(b).

6 Conclusion

In this work, I have shown on several examples that COMSOL Multiphysics is a valid tool for the modeling of plasmonic nanostructures with advanced functionality.

The topic of plasmonics was introduced, along with the necessary optical properties of metals and semiconductors. The Finite element method has been presented as tool for the modeling of structures with arbitrary shape. The modeling in COMSOL Multiphysics has been show in a tutorial manner, to allow readers to easily replicate and study the examples.

The examples shown are the typical components of plasmonics.

The Surface Plasmon Resonance in the prism coupled structures has been demonstrated in both Kretschman-Raether and Otto architecture, where both results were compared to analytical models. The Otto configuration has been extended for the use of InSb in the Terahertz regime, where a strong tuning of resonance using the magnetic field has been shown in the numerical simulation and compared to experimental data.

The ability of COMSOL Multiphysics to model planar waveguides has been illustrated on a plasmonic MIM waveguide.

One of the main contributions in the analysis of propagating modes on circular plasmonic waveguide, both in the dependence on the diameter of the waveguide and the wavelength (dispersion) on the gold nanowire. The propagation of surface plasmon has also been shown on InSb waveguide, along with symmetry breaking due to external magnetic field. This example provides an excellent testbed for the study of magneto-plasmons.

References

- [1] Jennifer A. DIONNE, *Flatland Photonics': Circumventing Diffraction with Planar Plasmonics Architectures*. Pasadena: California Institute of Technology, 2009.
- [2] Hans ZAPPE, *Fundamentals of Micro-Optics*. Cambridge: Cambridge University Press, 2010.
- [3] Rob P. H. KOOYMAN, "Physics of surface plasmon resonance," in *Handbook of Surface Plasmon Resonance*, pp. 15–20, RSC Publishing, 2008.
- [4] MAYSTRE, D., *Theory of Wood's Anomalies*. 2012.
- [5] Robert W. WOOD, "On a remarkable case of uneven distribution of light in a diffraction grating spectrum," *Philos. Mag*, vol. 4, pp. 396–402, 1902.
- [6] Mark L. BRONGERSMA and Pieter G. KIK, *Surface Plasmon Nanophotonics*, pp. 1–4. 2007.
- [7] J. C. Maxwell GARNETT, "Colours in metal glasses and in metallic films," *Philos. Trans. R. Soc. London*, vol. 203, pp. 385–420, 1904.
- [8] Gustav MIE, "Beiträge zur optik trüber medien, speziell kolloidalen metallösungen," *Ann. Phys.*, vol. 25, p. 377, 1908.
- [9] Rufus H. RITCHIE, "Plasma losses by fast electrons in thin films," *Phys. Rev.*, vol. 106, p. 874, 1957.
- [10] Rufus H. RITCHIE and E.T. ARAKAWA, "Surface-plasmon resonance effect in grating diffraction," *Phys. Rev. Lett*, vol. 21, pp. 1530–1532, 1968.
- [11] Andreas OTTO, "Excitation of nonradiative surface plasma waves in silver by the method of frustrated total reflection," *Z. Phys.*, vol. 216, p. 398, 1968.
- [12] Erich KRETSCHMANN and Heinz RAETHER, "Radiative decay of non-radiative surface plasmons excited by light," *Z. Naturf.*, vol. 23A, p. 2135, 1968.
- [13] William L. BARNES, Alain DEREUX and Thomas W. EBBSEN, "Surface plasmon subwavelength optics," *Nature*, vol. 424, pp. 824–830, 2003.
- [14] Lucia PETTI, Pellegrino MUSTO, "A plasmonic nanostructure fabricated by electron beam lithography as a sensitive and highly homogeneous SERS substrate for bio-sensing applications," *Vibrational Spectroscopy*, vol. 82, 2015.
- [15] Yiqin CHEN, Kaixi BI, Huigao DUAN, "Rapid focused ion beam milling based fabrication of plasmonic nanoparticles and assemblies via "Sketch and Peel" strategy," *ACS Nano*, vol. 10, pp. 11228—11236, 2016.
- [16] Xianmao LU, Matthew RYCENGA, Younan XIA, "Chemical synthesis of novel plasmonic nanoparticles," *Ann. Rev. of Phys. Chem.*, vol. 60, pp. 167–192, 2009.
- [17] KUHNE P., HERZINGER C. M., SCHUBERT M., WOOLLAM J. A. and HOFMANN T., "Invited Article An integrated mid-infrared, far-infrared, and terahertz optical Hall effect instrument," *Rev. Sci. Instrum.*, vol. 85, 2014.
- [18] Mostafa SHALABY, Marco PECCIANI, Yavuz OZTURK and Roberto MORANDOTTI, "A magnetic non-reciprocal isolator for broadband terahertz operation," *Springer Nature*, vol. 4, p. 1558, 2013.
- [19] O. STEPANENKO, T. HORAK, J. CHOCHOL, K. POSTAVA, J.-F. LAMPIN and M. VAN-WOLLEGHEM, "Compact mid-IR isolator using nonreciprocal magnetoplasmonic InSb mirror," in *2016 41st International Conference on Infrared, Millimeter, and Terahertz waves (IRMMW-THz)*, 2016.
- [20] Charles A. DIMARZIO, *Optics for engineers*. Boca Raton: CRC Press, 2012.

- [21] Matthew N. O. SADIKU, *Elements of Electromagnetics*. Oxford: Oxford University Press, 2015.
- [22] Kamil POSTAVA, “Thin films.” Presentation presented at Thin films course, 2010.
- [23] Heinz RAETHER, *Surface Plasmons on smooth and rough surfaces and on gratings*. Springer-Verlag Berlin Heidelberg, 2014.
- [24] H. A. LORENTZ, *Versuch einer Theorie der elektrischen und optischen Erscheinungen in bewegten Körpern*. Leiden: E. J. Brill, 1895.
- [25] Jan SOUBUSTA and Antonín ČERNOCH, *Optické vlastnosti pevných látek*. Olomouc: Univerzita Palackého v Olomouci, 2014.
- [26] David B. TANNER, *Optical effects in solids*. Gainesville: University of Florida, 2013.
- [27] Kamil POSTAVA, “Physical origin of material spectra.” Presentation presented at Spectroscopy of nanostructures course, 2010.
- [28] P. B. JOHNSON, R.W. CHRISTY, “Optical constants of the noble metals,” *Phys. Rev. B*, vol. 6, 1972.
- [29] Jan CHOCHOL, Kamil POSTAVA, Michael ČADA, Jaromír PIŠTORA, “Experimental demonstration of magnetoplasmon polariton at InSb(InAs)/dielectric interface for terahertz sensor application,” *Submitted in.*, 2017.
- [30] “The finite element method.” <https://www.comsol.com/multiphysics/finite-element-method>. Accessed: 2016-10-20.
- [31] Jianming JIN, *The finite element method in electromagnetics*. New York: Wiley, 1993.
- [32] Sara CARCANGIU, Augusto MONTISCI, Renato FORCINETTI, “Numerical simulation of wave propagation,” in *Ultrasonic Nondestructive Evaluation Systems*, pp. 17–26, Springer, 2015.
- [33] “Comsol multiphysics.” <https://www.comsol.com/comsol-multiphysics>. Accessed: 2017-04-06.
- [34] Ivan RICHTER, Pavel KWIECIEN, Jiří ČTYROKÝ, “Advanced photonic and plasmonic waveguide nanostructures analyzed with fourier modal methods,” *Transparent Optical Networks, 2013 15th International Conference*, 23-27 June 2013.
- [35] Jiří HOMOLA, *Surface Plasmon Resonance Based Sensors*. 2006.
- [36] Jiří HOMOLA, “Surface plasmon resonance sensors for detection of chemical and biological species,” *Chem. Rev.*, vol. 108, pp. 462 – 493, 2008.
- [37] G. GHOSH, “Dispersion-equation coefficients for the refractive index and birefringence of calcite and quartz crystals,” *Opt. Commun.*, vol. 163, pp. 95–102, 1999.
- [38] COMSOL, *RF Module User’s Guide*. 2012.
- [39] Diego Martin CANO, *Plasmonic waveguides: classical applications and quantum phenomena*. Madrid: Universidad Autónoma de Madrid, 2013.
- [40] Shinji HAYASHI and Takayuki OKAMOTO, “Plasmonics: visit the past to know the future,” *Jour. Phys. D*, vol. 45, 2012.
- [41] Sergey I BOZHEVOLNYI, *Plasmonic Nanoguides and Circuits*. Denmark: University of Southern Denmark, 2009.
- [42] Yurui FANG and Mengtao SUN, “Nanoplasmonic waveguides: towards applications in integrated nanophotonic circuits,” *Light: Science et Applications*, vol. 4, 2015.
- [43] Guo Ping WANG, Tadao SUGIURA, and Satoshi KAWATA, “Holography with surface-plasmon-coupled waveguide modes,” *Appl. Opt.*, vol. 40, 2001.

- [44] Sergei YUSHANOV, Jeffrey S. CROMPTON, Kyle C. KOPPENHOEFFER, “Plasmonic waveguide analysis.” Presented in: COMSOL Conference in Boston, 2015.
- [45] Yassin CHOWDHURY , *Plasmonic waveguides: design and comparative study*. Stockholm: Royal institute of technology, 2011.
- [46] M. A. ORDAL, R.J. BELL, R. W. ALEXANDER, L. L. LONG, M. R. QUERRY, “Optical properties of au, ni, and pb at submillimeter wavelengths,” *Appl. Opt.*, vol. 26, pp. 744–752, 1987.

